

The Ediacaran Salinas turbidites, Araçuaí Orogen, MG: tectonics and sedimentation interplay in a syn-orogenic basin

Felipe Garcia Domingues da Costa^{1,2*} , Fernando Flecha de Alkmim¹,
Pierre Muzzi Magalhães²

ABSTRACT: *The Ediacaran Salinas Formation exposed in the northern Araçuaí orogen is made up of syn-orogenic turbidites deposited between 580 and 560 Ma. Aiming to investigate how tectonic and sedimentary processes interact during the development of a flysch basin, we carried out a detailed field-based sedimentological and stratigraphic investigation of the Salinas Formation in its type-area located in northern Minas Gerais. Lithofacies and lithofacies assemblages recognized in the unit represent proximal to distal turbidite fan deposits, all of them affected by soft-sediment deformation. Based on the amount of lateral displacement and sediment volume involved, we distinguished four classes of soft-sediment deformation structures. The vertical facies changes of the whole Salinas Formation characterizes a coarsening-upward 1st-order sequence that record a general southwest-south progradation of a turbidite fan system fed from the north. The overall organization of the 25-60 m-thick fining-up cycles are especially elucidative of the interplay between tectonic and sedimentary processes during the accumulation of the Salinas turbidites. They initiate with thick sandstone beds deposited on top of intensively deformed strata, continuing with various sandy turbidite pulses, and ending with fine-grained sediments. In our view, they record the retraction and reorganization of the basin fill system after a sequence of seismic events.*

KEYWORDS: *Syn-sedimentary deformation; Araçuaí orogen; Salinas Formation; turbidite; tectonic and sedimentation.*

INTRODUCTION

Two categories of syn-orogenic basins, namely, fore-land and remnant ocean, are sites in which thick packages of turbidites can accumulate and be incorporated in the evolving orogenic edifice (*e.g.*, Ingersoll 2012, Allen *et al.* 2015). The turbiditic fill units of these basin types preserved in the Alpine and Apennine systems were originally referred to as *flysch* assemblages. Because of the geological setting and sedimentary processes associated with these successions, the term *flysch* was also used in the past to denote a tectofacies of the geosyncline cycle and, for a while, as synonymous of turbidites (see Mutti *et al.* 2009 for a comprehensive review). Besides the famous Alpine occurrences exposed in Switzerland and France, other examples of intensively studied syn-orogenic turbidite basins include the Proto-Adriatic basin in Northern Apennines, Italy, the Hecho Group in the Spanish Pyrenees, and Late

Paleozoic sequences of the Appalachian-Ouachita orogenic system in the United States (Mutti 1977, Ricci Lucchi & Valmori 1980, Shanmugam & Moiola 1988, Ingersoll *et al.* 1995, 2003, Mutti *et al.* 2009, Magalhaes & Tinterri 2010, Remacha & Fernández 2003, Cunha *et al.* 2017, Tinterri *et al.* 2016).

The Ediacaran Salinas Formation, made up of muddy, sandy and conglomeratic turbidites metamorphosed under greenschist to amphibolites facies conditions, occupies a relatively large area of the Araçuaí orogen located between the towns of Taiobeiras, Salinas, and Minas Novas in northern Minas Gerais (Pedrosa-Soares *et al.* 2001, 2008, Lima *et al.* 2002, Santos *et al.* 2009) (Fig. 1). Other small occurrences of the unit have been detected along a roughly NS-trend schist belt that extends between 18° and 21° South Lat in the central portion of the orogen (Peixoto *et al.* 2015). The Salinas Turbidites are currently interpreted as a flysch assemblage, accumulated during the final closure of

¹Universidade Federal de Ouro Preto – Ouro Preto (MG), Brazil. E-mails: felipe_garcia@petrobras.com.br, ffalkmim@gmail.com

²Petrobras – Rio de Janeiro (RJ), Brazil. E-mail: piermuzzi@petrobras.com.br

*Corresponding author.

Manuscript ID: 20180020. Received on: 03/02/2018. Approved on: 09/03/2018.

the Macaúbas basin (precursor of the Araçuaí orogen) in the course of the Brasiliano orogeny (Santos *et al.* 2009, Pedrosa-Soares *et al.* 2008).

How did tectonic processes control the accumulation of the syn-orogenic turbidites of the Salinas Formation? Having this question in mind we performed a detailed sedimentological and stratigraphic study in a representative section of the formation, which is exceptionally well exposed in a series of road cuts and quarries located between the towns of Taiobeiras, Salinas and Rubelita in northern Minas Gerais, the type area of the unit. This particular section comprises turbidites that preserve their typical sedimentary features, constituting thus the best site for the purpose of our investigation.

The present paper summarizes the results of our study on the Salinas Formation and aims to contribute to the understanding of the controls exerted by collisional tectonics on turbidite systems active in syn-orogenic basins. After describing and exploring the significance of lithofacies and soft-sediment deformation structures, the paper discusses vertical and lateral facies changes, and concludes with a model for the Salinas basin in the scenario of the development of the Araçuaí orogen.

GEOLOGICAL SETTING

The Brasiliano Araçuaí orogen, located between the São Francisco craton and the Brazilian continental margin, corresponds to approximately two thirds of a much larger tectonic feature, the Araçuaí-West Congo orogenic system (AWCO). Formed during the assembly of West Gondwana in the course of the Ediacaran and Cambrian periods, the AWCO also encompasses the West Congo belt of West-Central Africa (Pedrosa-Soares *et al.* 1992, 2001, 2007, 2008, Tack *et al.* 2001, Alkmim *et al.* 2006) (Fig. 1).

The Araçuaí orogen, consisting of an external fold and thrust belt and a crystalline core, is made up of the following lithotectonic assemblages (Fig. 1):

1. basement complexes composed of units older than 1,80 Ga;
2. Paleo/Mesoproterozoic rift-sag sequences of the Espinhaço Supergroup;
3. Tonian/Cryogenian Macaúbas Group and correlative units, representing rift to passive margin strata of the basin that closed to form the orogen;
4. 630–580 Ma granites of the pre-collisional G1 Supersuite, which together with coeval volcanosedimentary rocks form the Rio Doce magmatic arc;

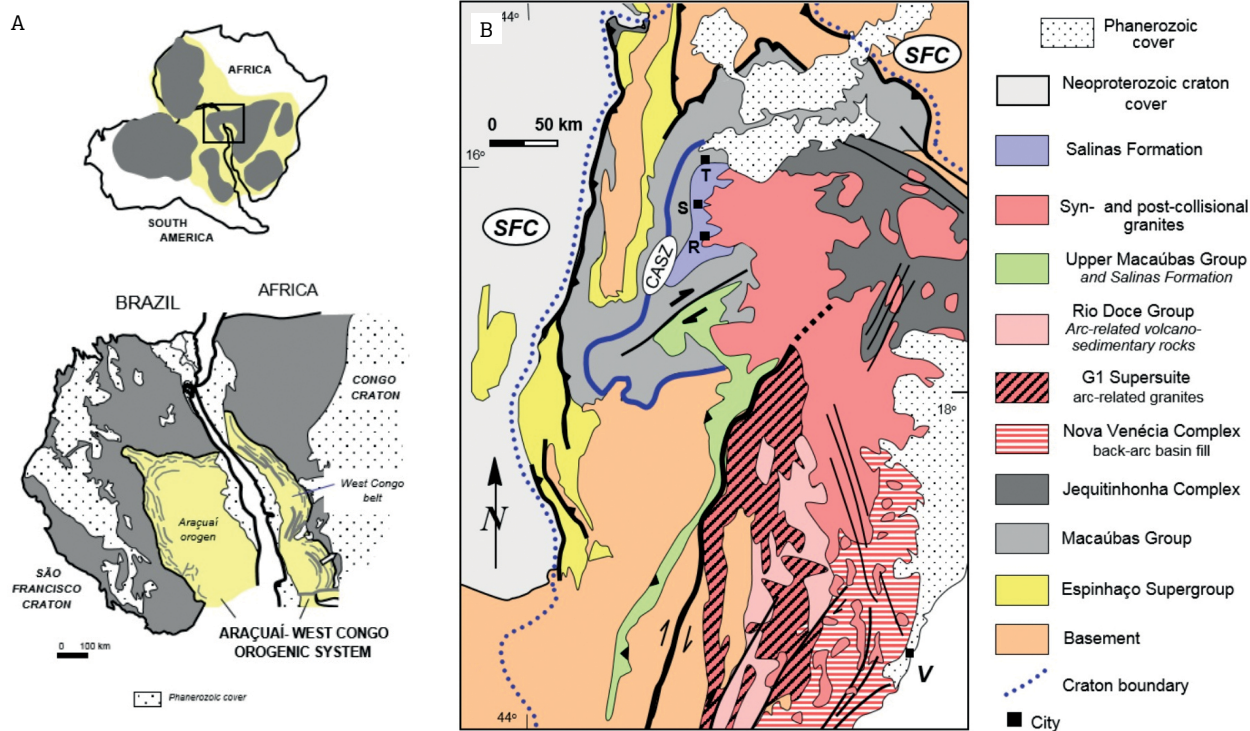


Figure 1. (A) The Araçuaí orogen as part of the Araçuaí-West Congo orogenic system, a component of the Neoproterozoic orogenic network of West Gondwana (South America and Africa). (B) Simplified geological map of the Araçuaí orogen. CASZ: Chapada Acauã shear zone; SFC: São Francisco craton. Cities: V: Vitória; T: Taiobeiras; S: Salinas; R: Rubelita.

5. paragneisses of the Jequitinhonha and Nova Venécia complexes, the latter representing an Ediacaran back-arc basin fill sequence;
6. 585–540 Ma syn- to late collisional S-type granites of the G2 and G3 Supersuites;
7. syn-orogenic turbidites of the Ediacaran Salinas Formation;
8. post-collisional granites of the 530–490 Ma G4 and G5 Supersuites (Pedrosa-Soares & Wiedemann-Leonardos 2000, Pedrosa-Soares *et al.* 2001, 2007, 2011, Gonçalves *et al.* 2016, Tedeschi *et al.* 2016).

The Salinas Formation occurs in the northwestern portion of the Araçuaí orogen in a large-scale synformal structure, partially bounded on the west and south by the Chapada Acauã normal sense shear zone and Minas Novas transpressional corridor, respectively (Fig. 1). In the remaining portions of its occurrence, the formation is separated from glacial and post-glacial units of the Macaúbas Group by a regional unconformity, and intruded by post-collisional granites of the G4-Supersuite (Pedrosa-Soares *et al.* 2001, Alkmim *et al.* 2007, Santos *et al.* 2009, Peixoto *et al.* 2018).

Pioneer studies on the Salinas Formation were carried out by Cobra (1970), Karfunkel *et al.* (1985) and Pedrosa-Soares *et al.* (1992), followed by more focused investigations conducted by Pedrosa-Soares (1995) and Pedrosa-Soares *et al.* (2001). Except for Cobra (1970), these authors described the metapelites and metawackes exposed near the town of Salinas in northern Minas Gerais as a distinct facies assemblage of the Macaúbas Group.

Lima *et al.* (2002) performed the first detailed sedimentological study on the Salinas Formation, identifying nine pelite, sandstone and conglomerate facies interpreted as turbidites accumulated in a deep sea fan and sourced essentially by a continental magmatic arc. The existence of an unconformity at the base of the formation and its lower metamorphic grade and internal strain, in clear contrast with the Macaúbas Group exposed in the adjacent areas, led Lima *et al.* (2002) to portray the Salinas Turbidites as a younger and late-orogenic succession. Furthermore, U-Pb SHIMP ages obtained by these authors on 13 detrital zircon grains indicated a maximum depositional age of ca. 568 Ma for the unit.

According to Santos *et al.* (2009), rocks of the Salinas Formation were affected by three phases of deformation. Elements of the first phase comprise a variety of soft-sediment deformation structures in association with growth strata. Structures of the second phase, coupled to a systematic WNW-directed tectonic motion and assisted by greenschist to amphibolite facies regional metamorphism, record the collisional stage of the Araçuaí orogen. The third phase was interpreted by the authors as a response to the emplacement of G4 post-collisional plutons, which induced deformation and contact-metamorphism in their vicinity. The Salinas

Formation was interpreted by Santos *et al.* (2009) as a syn-orogenic (flysch) assemblage, for the fact that it experienced the main collisional deformation and regional metamorphism. The anomalous low internal strain and metamorphic grade of Salinas Turbidites, which are on a first glance incompatible with its occurrence in the internal portion of the orogen, were explained by the authors as a result of ESE-directed normal motion along the Chapada Acauã shear zone (Marshak *et al.* 2006) that bounds the Salinas Formation to the west. During the extensional collapse of the orogen, the shear zone brought down a rock package that included the Salinas Formation and juxtaposed it with higher grade rocks of the Macaúbas Group (see also Peixoto *et al.* 2018).

Further estimations of the maximum depositional age of the Salinas Formation based on U-Pb geochronological determinations on detrital zircons and monazites, carried out by Pedrosa-Soares *et al.* (2008), Peixoto *et al.* (2015), Costa (2018), and Peixoto *et al.* (2018), resulted in the ages of 588 ± 24 Ma, 579 ± 11 Ma, 594 ± 10 Ma, and ca. 580 Ma, respectively. However, Kuchenbecker (2014) found 4 zircon grains in one single metasandstone sample with concordant ages around 548 Ma, considered by the author to represent the maximum depositional age of the Salinas Formation.

Another important outcome of the geochronological determinations carried out on detrital zircons extracted from the Salinas Formation was the characterization of its provenance. As pointed out by Pedrosa-Soares *et al.* (2008), Kuchenbecker (2014) and Costa (2018), the Salinas Turbidites must have been sourced mainly by the plutonic and volcanic rocks of the 630–580 Ma Rio Doce magmatic arc, exposed to the south and southeast of the Salinas Formation main occurrence area (Fig. 1).

The Macaúbas basin in its full development stage (Fig. 1), was a large gulf or inland sea connected to the Late Neoproterozoic Adamastor ocean that separated the São Francisco peninsula (currently represented by the São Francisco craton) from the Congo continent (the present-day Congo craton) (Pedrosa-Soares *et al.* 2001, 2008, Alkmim *et al.* 2006). The distal and largest portion of the basin was floored by oceanic crust, as indicated by the occurrence of ophiolites tectonically imbricate with passive margin deposits of the Upper Macaúbas Group in the southern half of the Araçuaí orogen (Pedrosa-Soares *et al.* 1992, 2001, Queiroga *et al.* 2007, Peixoto *et al.* 2015). However, during the deposition of the Salinas Turbidites, the ensialic sector of the Macaúbas basin started to be inverted and most of its oceanic segment had been already consumed under the 630–580 Ma Rio Doce continental margin arc (Santos 2007, Peixoto *et al.* 2015, Alkmim *et al.* 2007, 2017). The Macaúbas gulf was then converted into the Salinas basin, a remnant ocean basin *sensu* Ingersoll (2012).

METHOD

Our detailed sedimentological study was carried out in 25 stations (road cuts and quarries) located in the region between the towns of Taiobeiras, Salinas and Rubelita (Fig. 2).

Six of these stations correspond to large cuts of the BR-251 road, which expose continuous 33.0 to 179.0 m-thick intervals of a 1,830 m-thick section of the Salinas Formation. As shown in the schematic structural map and section of Figures 2B and 2D, the measured intervals are located in the hinge zones

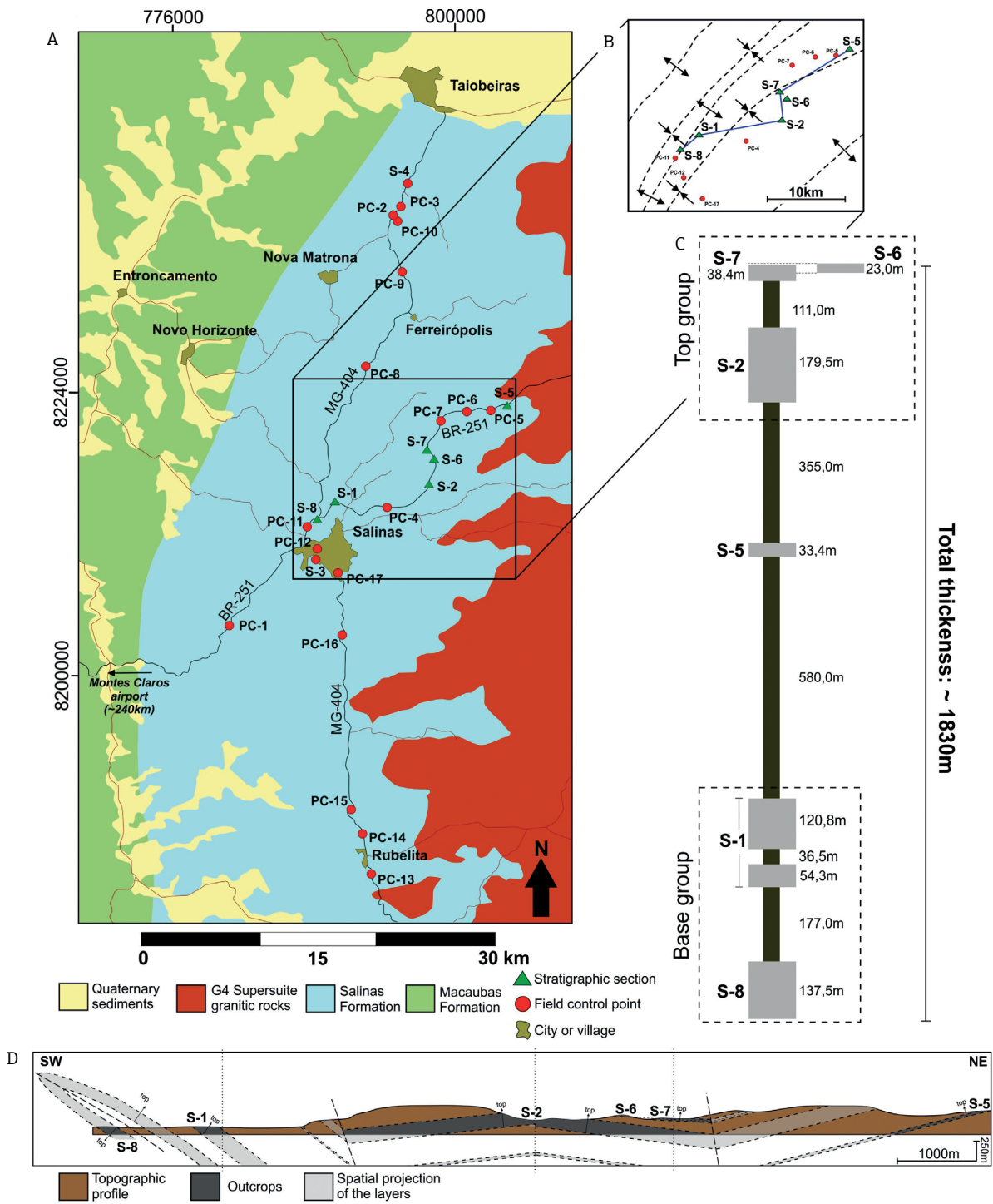


Figure 2. (A) Spatial distribution of the field stations. (B) Simplified structural map and the geological section on the map. (C) Schematic stratigraphic column showing the exposed and the covered parts of the rocks on the field. (D) Geological section showing the stations' distribution and the interval of exposed rocks.

of two adjacent NE-plunging regional folds. Along these zones, the beds show shallow dips and are almost free from the effects of orogenic deformation. Individual lithofacies and soft-sediment deformation structures were carefully described. Paleocurrents and kinematic indicators related to soft-sediment deformation structures were also documented.

As demonstrated by Talling (2001), Ricci Lucchi & Valmori (1980), Talling *et al.* (2007) and Remacha & Fernández (2003), the grain-size of a turbidite bed is related to its thickness. Knowing that the grain-size of the Salinas turbidites was modified by dynamic recrystallization during the syn-collisional metamorphism (Pedrosa-Soares *et al.* 2001, Lima *et al.* 2002), we compare the grain-size/thickness plots of the Marnoso-Arenacea Turbidites (Oligocen-Miocen, Northern Apennines) obtained by Talling (2001) and Ricci Lucchi & Valmori (1980) with our data. As expected, quartz and feldspar grain-size were reduced, whereas the original clays, replaced by biotite and white mica, experienced a considerable enhancement. Despite these effects, the aforementioned relationship is maintained, and the studied intervals were equally affected by metamorphic processes, so that we could describe the Salinas lithofacies in the same way as their

sedimentary equivalents. Of note, preservation of the finest details of the sedimentary features (see photos in the next sections) is one the most remarkable aspects of the Salinas Formation in its type locality.

LITHOFACIES AND LITHOFACIES ASSEMBLAGES

Eight distinct sedimentary facies were discriminated based on grain size and sedimentary structures in the exposures of the Salinas Turbidites. Among these, five occur in close association with other lithofacies, characterizing two distinct assemblages described in the next sections and summarized in Table 1. The codes used for the individual lithofacies and lithofacies assemblages are according to Mutti *et al.* (1999, 2009).

Conglomerates (F3)

Thick sections of clast-supported conglomerates interbedded with sandstones (Fig. 3A) occur in the vicinity of the town of Taiobeiras in the northern portion of the study area.

Table 1. Summary of described facies, sedimentary processes and architectural elements of the Salinas Formation.

Facies	Code	Description	Sedimentary process	Architectural element
Conglomerates	F3	Metric beds of clast-supported conglomerates containing boulder-sized sandstone intraclasts, sandstone intercalations, and long-axis imbrication of lithic cobbles and pebbles.	Gravel bars deposited by density flows	Feeder channels in transfer zone
Intraclastic breccias	F5	Lenses and beds of angular fragments of deformed sandstones and pelites dispersed in a fine grained sandstone matrix	Clasts generated and captured by density flow impact on obstacles or Dismembered slump sheets and incorporation in density flows	Channel fill inside the turbidite system transfer zone
Graded sandstones		Metric beds of coarse- to fine-grained sandstones arranged in normal-grading cycles, showing erosional sharp base, pelitic intraclasts and water escape structures	Quickly deposition by a granular flow, confining fluids in a high pore pressure strata	
Cross-bedded Sandstones	F6	Decimeter-thick beds of coarse- to medium-grained sandstones exhibiting mega-ripple through cross-bedding that occur on top of graded sandstones	Reworking of density flow deposits by the turbulent upper flow	Boundaries between turbidite system transfer zone and accumulation zone
Massive sandstones	F8	Centimeter- to meter-thick beds of homogenous fine- to medium-grained sandstones showing erosional sharp base and load casts	Laterally compensated sand lobes deposited by density flows	Sand lobe accumulation zone
Sandstones with ripples	F9	Centimeter-thick layers of fine-grained sandstones and pelites containing ripples and climbing ripples. In this facies, cross-lamination are well preserved	Sedimentation through traction-plus-fallout processes. Traction dominant	Basin plain
Laminated sandstones and pelites		Centimeter to decimeter-thick layers of interbedded fine-grained sandstones and pelites showing planar laminations	Sedimentation through traction-plus-fallout processes. Fall-out dominant.	
Laminated pelites		Millimeter to meter-thick layers of pelites showing planar laminations	Fall-out process dominant	

The conglomerates are poorly sorted and in general unstratified. When present, the stratification is marked by a diffuse inverse gradation or thin sandstone intercalations. Well rounded, pebble- to boulder-sized lithic clasts are immersed in a fine- to medium-grained sandy matrix. Clasts of granites and acid volcanic rocks predominate. Quartzites, schists, vein-quartz, and minor carbonates clasts also occur. Bolder-sized intraclasts of deformed sandstones containing pebbles and cobbles were also often observed.

A remarkable feature exhibited by all conglomerates is the long-axis imbrication of their clasts (*i.e.*, a(p) a(i)-imbrication *sensu* Harms *et al.* 1975) (Fig. 3B). The clast long-axes define a lineation preferentially oriented at 040/35, characterizing thus S40W as the dominant flow direction (Fig. 4A). Although the number of effective data measured is low, the data acquired are consistent because the conglomerates outcrops exposures is quite large (located mainly in a closed mining field) and

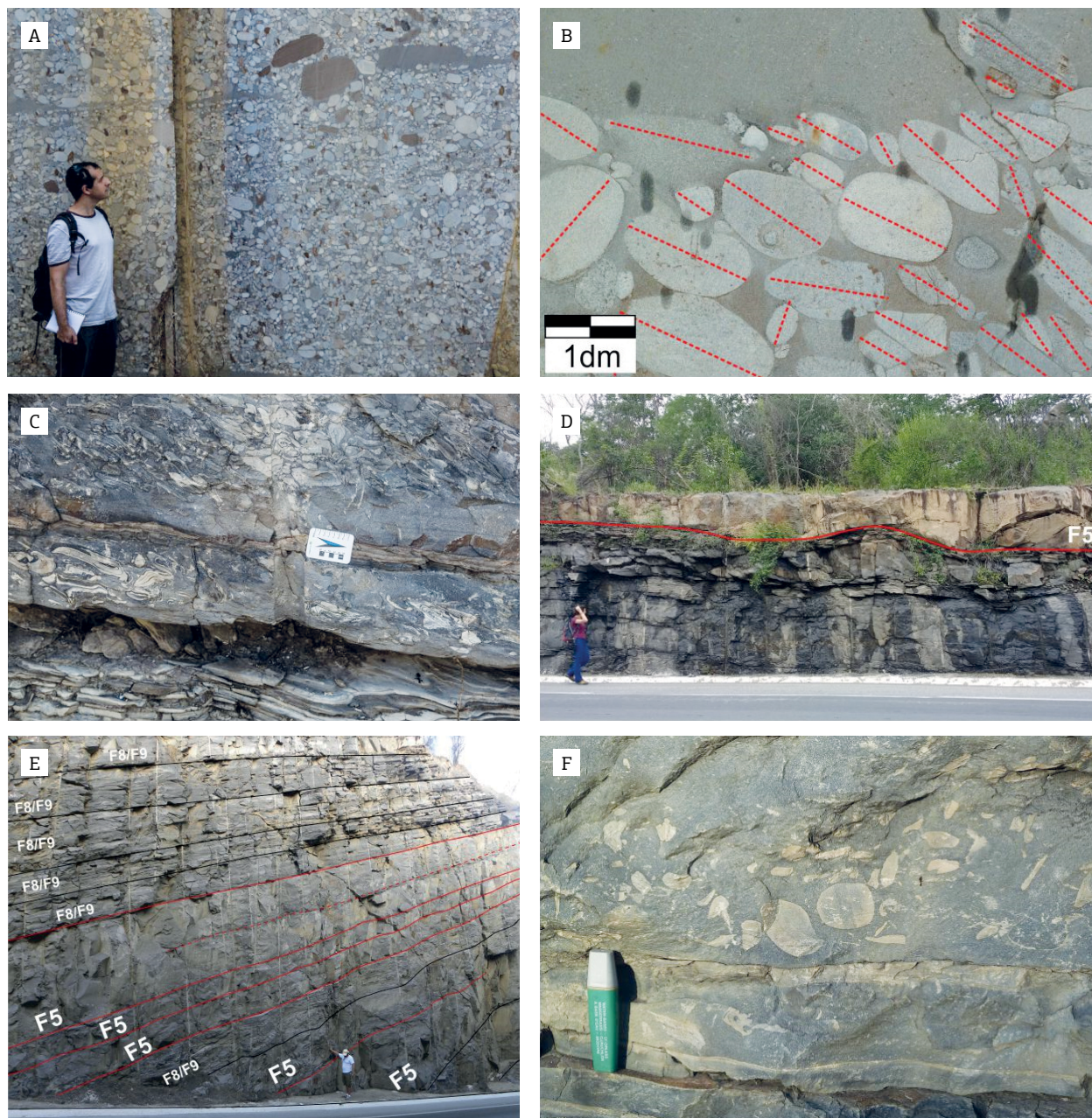


Figure 3. (A) Clast-supported conglomerates (F3). (B) Long-axis imbrication of the conglomerates clasts. (C) Two layers of intraclastic breccias (F5) showing clasts totally deformed. (D) Deformed base of the graded sandstone (F5) strata. This deformation probably occurred during the quickly deposition of the graded sandstone over thin and underconsolidated strata. (E) Large exposure of graded sandstones layers (F5) in direct contact with other thin-layered facies. (F) Dispersed intraclasts in the basal portion of the graded sandstone (F5).

a visual control of this data dispersion was made during data collection.

Conglomerates with distinct structures and textures characterize proximal deposits of the turbidite fan systems (Walker 1975, 1992, Mutti 1992, Mutti *et al.* 1999). Specifically, poorly-sorted, coarse-grained, unstratified or inversely graded conglomerates with imbricate clasts characterize the deposits of the basal planar density flows, accumulated in form of bars in the system feeding channels (Mutti *et al.* 1996).

Intraclastic breccias (F5)

Breccias made up of fine-grained sandstones and pelite intraclasts containing a medium to coarse-grained sandy matrix occur in the form of lenses intercalated with graded sandstones beds. They show sharp scoured bases and thicknesses varying between 0.2 and 1.5 m. The pebble- to boulder-sized intraclasts are deformed and imbricated (Fig. 3C).

For Magalhaes & Tinterri (2010), Tinterri & Magalhaes (2011) and Amy *et al.* (2005), the incorporation of clasts removed from the bottom irregularities by the action of dense flows is the process that led to the generation of the

intraclastic breccias associated with graded sandstones. Alternatively, we suggest that these breccias could also be generated by the full disaggregation of slump sheets (see next section). The produced fragments would be subsequently captured by dense flows, as indicated by their imbrications. In favor of our hypothesis, we observe the presence of intensively deformed clasts and the sharp contacts of these breccias.

Graded sandstones (F5)

Centimeter- to meter-thick beds (Figs. 3D and 3E) of poorly sorted, very coarse- to medium-grained sandstones showing normal gradation characterizes this lithofacies. The base of the beds is often erosive and associated with flute casts, groove marks and water escape structures. Their upper portions are marked by abrupt contacts or transitions into massive sandstones (F8 facies) and, less frequently, to sandstones with ripples, and interbedded sandstones and pelites (F9 facies). Well-rounded to angular intraclasts of fine-grained sandstones and pelites dispersed in the basal portion of the strata were often observed (Fig. 3F). As mentioned before, lenses and beds of intraclastic breccias also occur in association with this lithofacies.

In the models of Mutti *et al.* (1999, 2003), graded sandstones are portrayed as deposits of the transition zone between channels and sand lobes of the turbidite system. Due to the decrease in the slope angle that characterizes the transition zone, deposition of these sands is very fast, causing liquefaction and fluidization of the underlying strata.

Paleocurrent data from sole marks associated with graded and massive sandstones (F8 facies, see below) are plotted together in the diagram of Figure 4B. They indicate S32W as dominant flow direction, compatible with the direction obtained from imbricate conglomerate clasts (Fig. 4A).

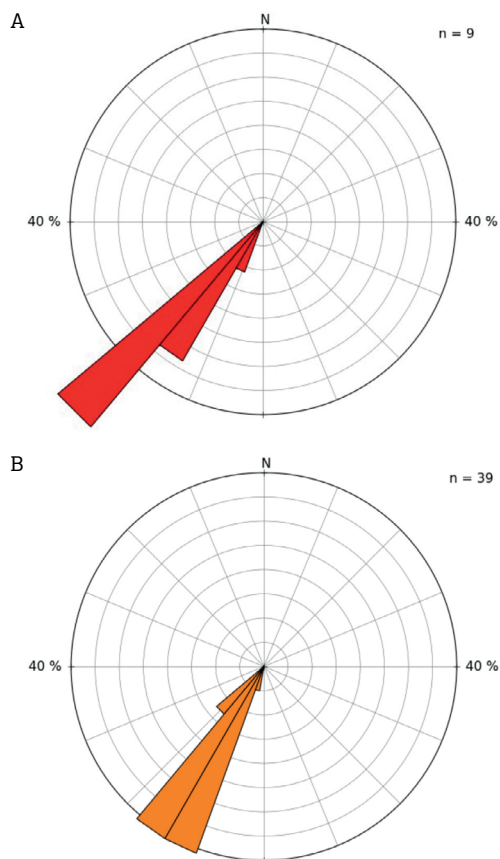


Figure 4. (A) Rose diagram showing the paleocurrent data as indicated by imbricated clasts from conglomerates facies (F3). (B) Rose diagram showing the paleocurrent indicated by sole marks associated with the graded sandstone facies (F5).

Cross-bedded sandstones (F6)

Tangential cross-bedded sandstones are rare in the described sections. When present, they occur in form of 10 to 80cm-thick beds of very coarse- to coarse-grained sandstones showing trough and less frequently tabular cross-bedding (Figs. 5A and 5B). Following Mutti *et al.* (1999), we interpret this lithofacies as the last product or the granular density flow along its down slope motion, also accumulated in the channel-lobe transition zone. For D'Ávila *et al.* (2008), cross-bedded sandstones reflect the action of very turbulent and long-lived flows, which exert significant traction on the sandy substrate.

Massive sandstones (F8)

Massive sandstones are by far the most abundant lithofacies in the sections we have described. They occur in the form of centimeter- to meter-thick strata of medium- to fine-grained sandstones, often showing sole marks (Fig. 4B), water escape structures, and always associated with members

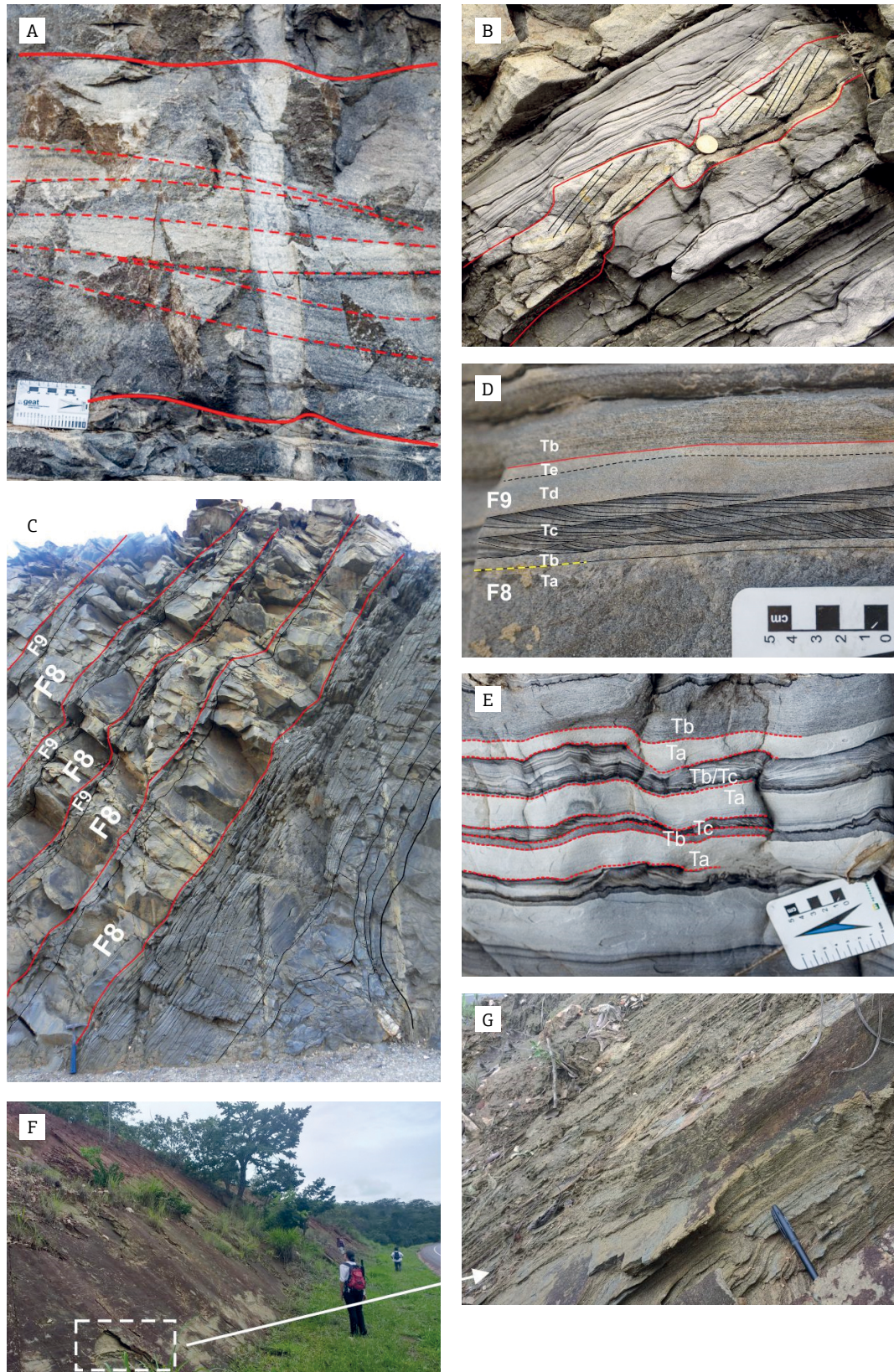


Figure 5. (A) Cross-bedded sandstone (F6) exhibiting large oblique stratifications. (B) Deformed cross-bedded sandstone between thin layers. (C) Association between massive sandstone (F8) and other thin lithofacies. (D) Contact between facies F8 and F9, showing a complete scheme proposed by Mutti et al. (1999) and Bouma (1962). (E) Lithofacies association between fine sandstone and pelites arranged in planar and cross-bedded laminations (facies F9). (F) Outcrop showing laminated pelite sequences (F9). (G) Detail of the pelite lamination.

of the F9 lithofacies assemblage (see below and Table 1) (Fig. 5C). Their upper boundaries can be planar or undulated.

Graded and massive sandstones form the basal Ta interval of the classical Bouma sequence (Bouma 1962), which in later published models is portrayed as sand lobes accumulated in the mid-fan zone by turbulent flows associated with a near bed suspension (Middleton & Hampton 1973, Mutti *et al.* 1999, D'Ávila *et al.* 2008).

Sandstones with ripples, intercalated sandstones and pelites, laminated pelites (F9)

Due to their effective association, these individual lithofacies are here grouped in the assemblage F9, as in the facies models developed by Mutti (1992) and Mutti *et al.* (1999, 2003, 2009).

Sandstones with ripples and climbing ripples are medium- to fine-grained and occur in the form of 5 to 80 cm-thick strata and intercalated with laminated sandstones and pelites on top of the massive sandstones (Figs. 5D and 5E). The members of this lithofacies assemblage are very frequently affected by a variety of soft-sediment deformation structures, as described in the next section.

In the measured sections, the laminated pelites occur only intercalated with sandstone laminae. However, as observed in outcrops in the southern portion of the study area and well documented in the literature, the basal portion of the unit consists essentially of fine-laminated pelites containing small lenses and thin beds of marls (Figs. 5F and 5G). Metamorphosed into biotite garnet schists, these rocks dominate the exposures of the Salinas Formation south of the town of Rubelita (Fig. 2) (Pedrosa-Soares *et al.* 2001, Lima *et al.* 2002, Santos *et al.* 2009).

The assemblage of F9 lithofacies correspond to the Tb, Tc and Td intervals of the classical Bouma sequence. Similar facies assemblage documented in turbidite systems of passive margin basins were interpreted as deposits of levee-channel complexes by Walker (1992). In the models by Mutti (1992) and Mutti *et al.* (1999) for confined turbidite systems, the F9 assemblage represents deposits of the turbulent upper flow in the more distal portions of the lobes and basin plains, where pelagic fallout also occurs.

The paleocurrent directions obtained from ripples of the F9 lithofacies define a bimodal distribution with relatively great dispersions around S55°E, the main direction, and S70°W (Fig. 6). A comparison of diagrams of Figures 4 and 6 shows that the main vector obtained from ripples is orthogonal to the flow direction indicated by the sole marks and imbricate clasts, which in turn diverge in 35° from the subordinate direction indicated by the ripples. This discrepancy in the orientation of the paleocurrent indicators can be observed even in beds that are only a few centimeters apart in vertical sections, as shown in Figure 7.

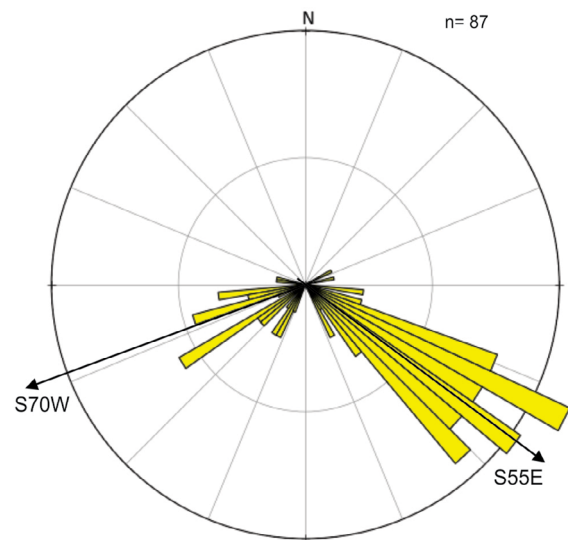


Figure 6. Rose diagram showing the paleocurrent data collected on the fine sandstones and laminated pelites facies (F9) from ripple marks.

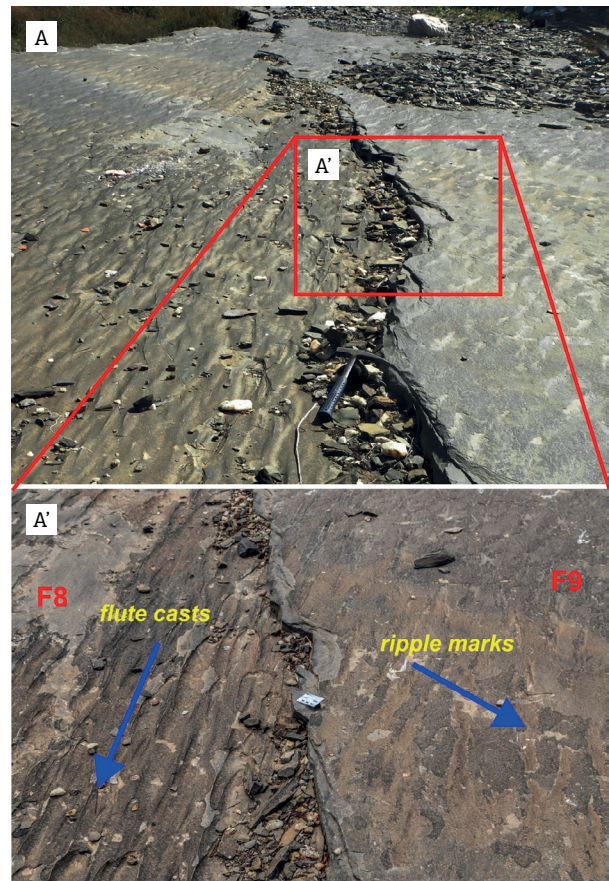


Figure 7. (A-A') Large outcrop exposure showing the oblique paleocurrent direction (blue arrows) between flute casts in the base of a massive sandstone (F8) and ripple marks in the top of laminated sandstones and pelites (F9).

Imbricate clasts and sole marks are paleocurrent indicators of high accuracy and low variability, reflecting the dense flow along the highest slopes of the basin floor (Miall 1990, Potter & Pettijohn 1977, Graham 1988). Ripples, on the other hand, as bed forms of turbulent tractive flows, are largely influenced by local factors, providing current directions of lower accuracy and high variability. Because of that, we assume that the main current direction during the sedimentation was towards south-west, following the NE-SW oriented axis of the Salinas basin.

SOFT-SEDIMENT DEFORMATION STRUCTURES

Strata of all previously described lithofacies show deformation structures that predate the collisional deformation phase of the Araçuaí orogen, as documented by Santos *et al.* (2009). These structures affect mainly the finer-grained rocks of

lithofacies F8 and F9, are confined to specific beds, and associated with growth features in most cases. Developed immediately below the depositional surface and preceding any diagenetic processes, these features record multiple events of soft-sediment deformation (*sensu* Rosseti 1999, Owen *et al.* 2011, Moretti & Sabato 2007, Tinterri *et al.* 2016).

The soft-sediment deformation structures documented in the Salinas Formation define a broad spectrum of features, which reflect increasing motion of the strata involved. The end members of this spectrum are represented by undeformed strata and intraclastic breccias. According to the nature and amount of lateral displacement, these structures were grouped into four classes, as follows (Fig. 8):

1. Class 1: Water-escape structures;
2. Class 2: Slightly deformed depositional and post-depositional structures;
3. Class 3: Folds and faults;
4. Class 4: Chaotic strata.

	Soft-sediment deformation structures	Driving-force system	Triggering mechanism
Class 1		Gravitational unstable density gradient and/or Lithostatic pressure rebalancing Local extensional stress	Overloading Strata accommodation or earthquake?
Class 2		Shear stress	Overloading or earthquake
Class 3		Shear stress	Earthquake
Class 4		Slump sheet	Earthquake

Figure 8. Diagram showing a panorama of the syn-sedimentary deformation structures observed in the Salinas rocks assemblage, their distribution in four classes of the intensity deformation, the deformation driving-force systems and the triggering mechanisms interpreted for each class.

Water-escape structures

A large variety of water-escape structures occur in the described sections of the Salinas Formation. The most common type of these features are flame structures, which occur in form of 1 to 80 cm-high pelitic injections into sand beds of facies F5 and F8 (Fig. 9A). Other features of this class are pseudo-nodules, balls and pillows, dishes, pillar structures and mushroom-like protrusions of pelites into sandstones (Figs. 9B, 9C and 9D).

As pointed out by various authors, the development of these structures requires rapid sedimentation and entrapment of a considerable amount of water in the intergranular space, followed by the action of a triggering mechanism, as discussed at the end of this section (Potter & Pettijohn 1977, Bosellini *et al.* 1989).

Other structures of this category are clastic or neptunian dykes. Very rare in measured sections, they occur in the form of wedge shaped, cm- to dm-sized wide cracks filled by fragments of the above laying strata. The upper portions of the dykes are in general bounded by series of small normal faults (Fig. 9E).

All structures ascribed to this class are symmetric, i.e., they show an orthorhombic symmetry in vertical sections and are not associated to any visible lateral motion, being thus considered autochthonous. This fact implies that their generation occurred essentially under a pure shear stress regime.

Slightly deformed depositional and post-depositional structures

This category comprises all structures of class 1, which underwent significant shearing, exhibiting thus a clear asymmetry. The sense of shear deduced from these features is always compatible with the vergence of classes 3 and 4 structures affecting strata nearby. Examples of class 2 structures are asymmetric open folds, sheared balls and pillows, pseudo-nodules, and load cast ripple marks (Figs. 9F, 9G and 9H).

Folds and faults

Confined between undeformed strata, centimeter- to meter-thick individual beds or bed sets are affected by thrust faults and asymmetric folds and, less frequently, by normal faults. Together, all these structures have been developed during motion of relatively larger masses of soft sediments, and as such seem to represent the internal fabric elements of slump sheets.

The folds are closed to isoclinal and in general asymmetric. They occur in centimeter- to outcrop-scale as isolated elements or in fold trains, associated or not with faults. The thrusts faults also occur in form of small- to large-scale features, showing the same sense of motion indicated by the vergence of the associated folds. Normal faults were only observed in a few places affecting centimeter-thick strata.

The slumped beds as a whole and their internal structures created highs and lows in the depositional surface. The lows,

represented by synclines, bounded or not by thrust faults, are filled by subsequent turbiditic deposits, giving rise to a large variety of growth features, as illustrated by Figures 10A, 10B, 10C and 10D.

Folds and thrusts exhibit a strong preferential orientation. They trend N37E and verge preferentially southeast (Fig. 11). Only a few cases of NW-vergence were observed.

Chaotic strata

Some intervals of the investigated sections show thick beds (up to 50 m-thick) of fully contorted strata bounded by undeformed layers. Internally, they show complex folds and faults (Figs. 10E and 10F). Despite their chaotic nature, they represent a coherent rock mass, differing from intraclastic breccias end member mainly by the absence of a matrix separating loose rock fragments. In our view, the intraclastic breccias very likely correspond to the most intensively deformed and disaggregated portions of slumps. This relationship was, however, not observed in outcrops, due to the spatial limitation of exposures in the study area.

Driving forces, causative mechanisms and triggers of the soft-sediment deformation

The pre-orogenic deformation features documented in the Salinas Formation clearly resulted from a fast decrease in the shear strength of the sediments immediately after their deposition. Fast deposition (causing water saturation of the pore space), liquefaction, and fluidization are the processes involved in the generation of soft-sediment deformation structures (Allen 1984). The triggering mechanism for liquefaction and fluidization and generation of the class 1 observed structures is, however, a matter of a longstanding debate in the literature. Overloading, differential loading, sudden changes in the ground-water level, earthquakes, and wave-induced stresses are currently invoked by the authors as possible triggers (see, among others, Rosseti 1999, Allen 1980, Moretti & Sabato 2007, Owen & Moretti 2011, Owen *et al.* 2011, Shanmugam 2017).

Except for the clastic dykes, structures of classes 1 and 2 in turbidites are commonly interpreted as product of overloading of water saturated sediments (Tinterri *et al.* 2016, Owen 2003). Fast deposition of thick turbiditic strata on top of sediments of the same nature can induce their liquefaction and fluidization. As pointed out by Tinterri *et al.* (2016), another possible causative mechanism is wave impact. Especially in tectonically controlled depositional settings, reflections of the upper turbulent flows on obstacles can enhance water waves and their impact on the substrate, inducing the generation of overpressurized zones and their subsequent deformation. Therefore, all these processes are



Figure 9. (A) Pelitic flame structures penetrating the base of the massive sandstone (F8) by overloading process. (B) Deformation structures like a ball and pillows and pelitic pseudonodules inside the fine sandstone facies F8 and F9. (C) Accommodation of the pelitic pillows formed by the vertical movement of the sand during the water escape process. (D) Vertical conducts formed by the water escape process inside the sandstone facies F8. (E) A set of small blocks of laminated rocks filling the clastic dyke. Note that each block has a different spatial orientation. (F) Sheared balls and pillows showing vergence. (G) Oriented deformation of the massive sandstone (F8) forming convolute folds. (H) Intense deformation on the top of the massive sandstone (F8) strata establish a set of sheared balls and pillows.

endogenic (Owen & Moretti 2011, Owen *et al.* 2011) and often documented in turbidite successions.

Clastic dykes, representing open tensile fractures filled with fragments of the beds involved, are currently viewed as a response to extensional stresses acting upon cohesive sediments (Moretti & Sabato 2007). They may be formed in the proximal and upper portions of slump sheets, which in turn can be triggered by seismic events.

Structures of classes 3 and 4, as well as large-scale features of class 2 affect bed sets over relatively larger areas and are quite frequent in the studied sections. They meet the criteria listed by Owen & Moretti (2011) to be related to external driving forces and probably to seismic triggers. As fabric elements of slumps sheets (see Owen *et al.* 2011), these structures record successive mass motions towards southeast, as indicated by their vergences. This sense of motion is however orthogonal

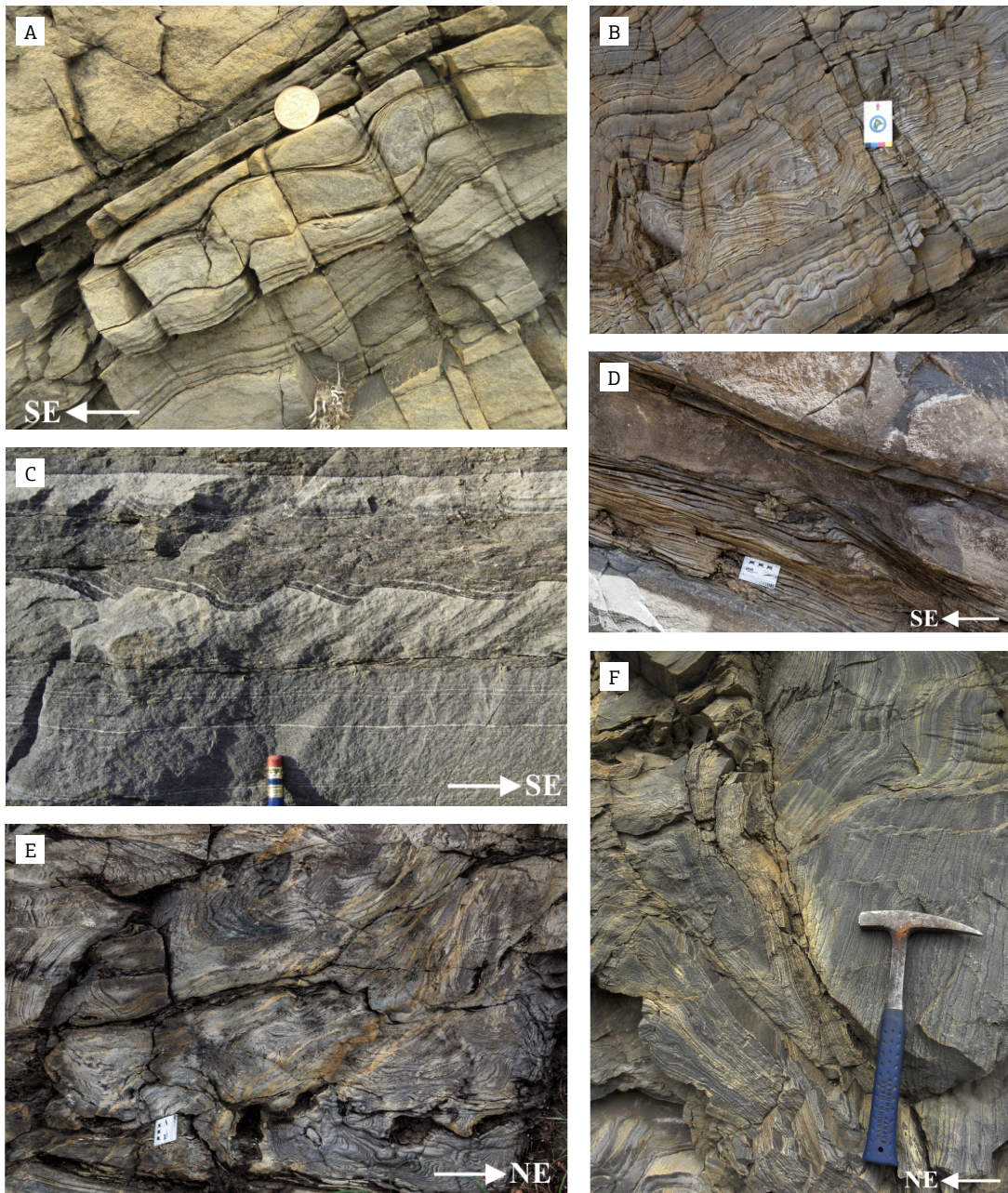


Figure 10. (A) Syn-sedimentary folds and sedimentary pelitic growth in a thin sandstone layer. (B) Slumped beds of laminated sandstones and pelites between a set of undeformed strata or displaying a different pattern of deformation. (C) Facies F9 deposits affected by normal faults and exhibiting growth strata. The deformed sedimentary successions are enclosed by undeformed strata. (D) Bottom irregularities formed by the deformational structures and covered by a differential sedimentation pattern. (E and F) Chaotic strata displaying a complete disorganization of internal layers patterns.

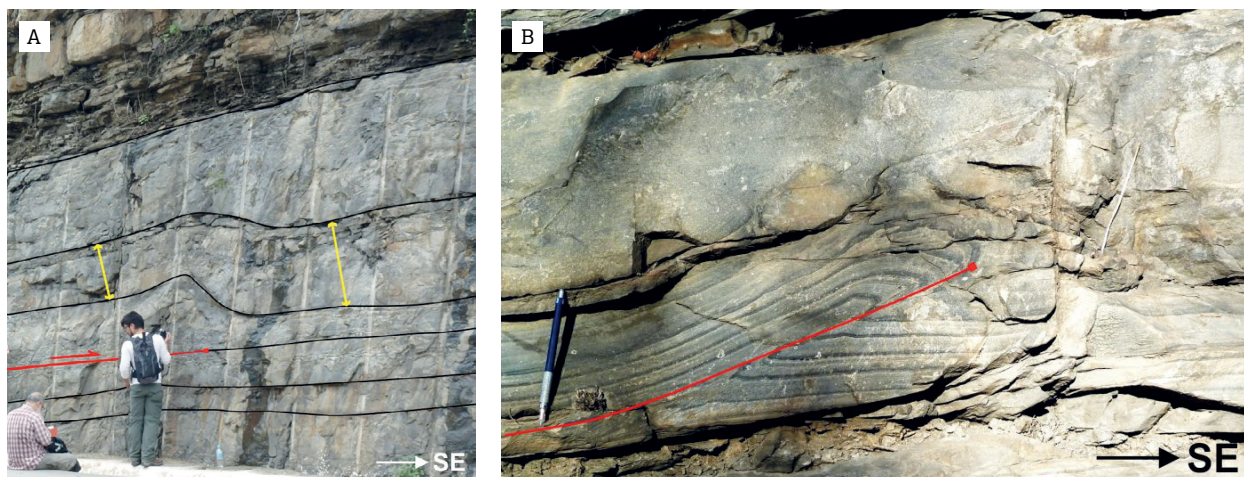


Figure 11. (A) Metric-thick strata facies F8 deposited above a bottom irregularity formed by a thrust fold structure. (B) Centimetric thrust fault and related fold affecting fine sandstones and laminated pelites (F9) and covered by a massive sandstone (F8).

to the paleocurrents deduced from sole marks and imbricate clasts, but coincident with the main transport direction obtained from ripples, suggesting that a considerable topographic relief marked the cross sections of the Salinas basin. Thus, along SE-inclined ramps, large sediment masses probably became often unstable and slid down.

LATERAL AND VERTICAL FACIES VARIATIONS

Lateral facies changes

The exposures in the study area are limited and do not allow the mapping of individual beds over distances larger than a road cut outcrop. Because of that, we could not document lateral facies changes in individual beds. However, our observations in the various stations in the study area together with literature data suggest that the facies distribution related to a single turbiditic flux along the NE-SW trending axis of Salinas basin occur in the form, as illustrated in Figure 12. F3 facies conglomerates and subordinate F5 facies sandstones predominate in the north, near the town of Taiobeiras, characterizing thus the most proximal domain of the system preserved in the Salinas Formation. Towards southwest, the conglomerates would grade into the F5 facies. The F8 and F9 lithofacies dominate the various exposures in the vicinity of Salinas, whilst the F9 laminated pelites are the more abundant lithofacies in areas farther south.

In order to characterize the geometry of the F5/F8 facies sandstones, we also have documented their thickness variations across the basin axis. For this purpose we examined exposures located in opposite sides of Route BR 251. Even over such short

distances, the thickness of the sandstone beds varies significantly, reflecting their lobate geometry and therefore important facies changes across the basin axis. Furthermore, we estimated the minimum lateral extension of the sand bodies based on bed thickness, bed surface angle and distance between measurement stations. The results we obtained indicated minimum widths between 50 and 70m for the sandstone bodies of section 2 (Fig. 2) and between 90 and 130m for the section 7.

Vertical facies changes

As documented by Santos (2007) and Santos *et al.* (2009), the Salinas rocks occur inside a NE-plunging synclinorium, in which the fine-grained lithotypes occupy the south side and limbs, and coarser rocks its central and northern portions. These facts led to the conclusion that the Salinas Formation comprises an overall coarsening-upward and progradational succession (Fig. 13). This succession seems to represent a complete basin-fill and thus an unconformity-bounded 1st-order sequence (*sensu* Catuneanu 2005).

The sections we investigated in detail belong to the middle Salinas Formation. As previously mentioned, these sections together with the covered or poorly exposed intervals encompass c. 1,830 m of turbidites of a total thickness that probably exceeds 3,600 m. They consist of c. 150 m-thick coarsening and fining-up successions, which in turn encompass 25–60 m-thick fining-up cycles. Cyclic successions with average thicknesses of 8.0 and 1.2 m, respectively, always exhibit fining upward patterns (Fig. 14).

Figure 15 illustrates the typical stacking pattern of the Salinas 25–60 m-thick fining upward successions. In general, they initiate with high-energy turbiditic events, represented by deposits of relatively thick beds of the F5/F8 lithofacies, which follow important soft-sediment deformation episodes,

recorded by class 4 or 3 soft-sediment deformations. In the example of Fig. 15, the 25–60 m-thick succession starts with three high-energy turbiditic events deposited on top of a thick bed of chaotic sandstones. Further upsection, after two more high-energy events succeeding intervals with class 3 soft-sediment deformation structures, the F9 lithofacies become predominant.

TECTONICS AND SEDIMENTATION IN THE SALINAS BASIN: A MODEL

The data and interpretations presented in the previous sections along with the available literature allow us to propose a model for a tectonically controlled accumulation of the Salinas Turbidites during the syn-orogenic development stage of the Araçuaí orogen.

The Salinas Turbidites were deposited in the Edicaran Period, between 580 and 560 Ma (Pedrosa-Soares *et al.* 2008, Peixoto *et al.* 2015, Costa 2018, Peixoto *et al.* 2018). At this time, the Macaúbas basin, in process of closure, was succeeded by the Salinas basin, a remnant of the preexistent gulf or inland sea (Pedrosa-Soares *et al.* 2008, 2011, Santos *et al.* 2009).

As postulated by Santos *et al.* (2009) and confirmed by our study, the Salinas basin, fed from the north-northeast, would correspond to a large and curved trough, open to south-southwest, and bounded to the east by an advancing tectonic wedge (Fig. 13). The turbidite fan system prograded toward southwest and south along the main depocenter fore-deep, as indicated by the paleocurrent data set, lateral facies

variations, and the coarsening-up pattern of the preserved Salinas 1st-order sequence. Moreover, the WNW-directed propagation of the thrust wedge, besides segmentation of the basin floor, might have imposed a pronounced asymmetry in the basin cross-sections, which probably consisted of long and shallower dipping ramp on the west and with a short and steep slope developed on the eastern orogenic wedge. Similar geometries are reported in various settings documented worldwide (Magalhaes & Tinterri 2010, Cunha *et al.* 2017, Romans *et al.* 2011).

In the basin scenario portrayed above, the controls exerted by tectonic processes upon the Salinas turbidite system are recorded especially by the 25–60-m-thick fining upward successions, which start with thick F5/F8 lithofacies beds

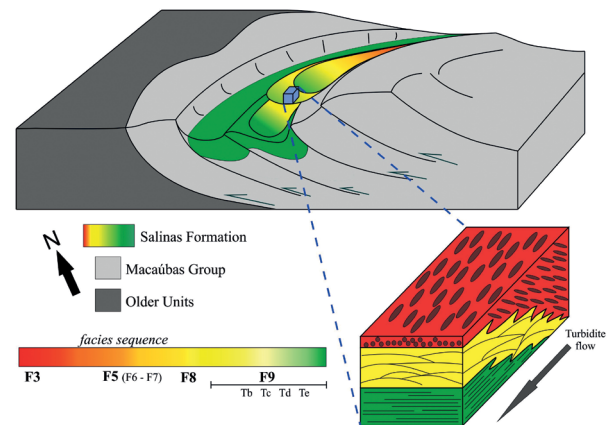


Figure 13. Structural 3-D model of the Salinas basin formation and basin-fill succession. Note the box showing the coarsening-upward first order sedimentary pattern.

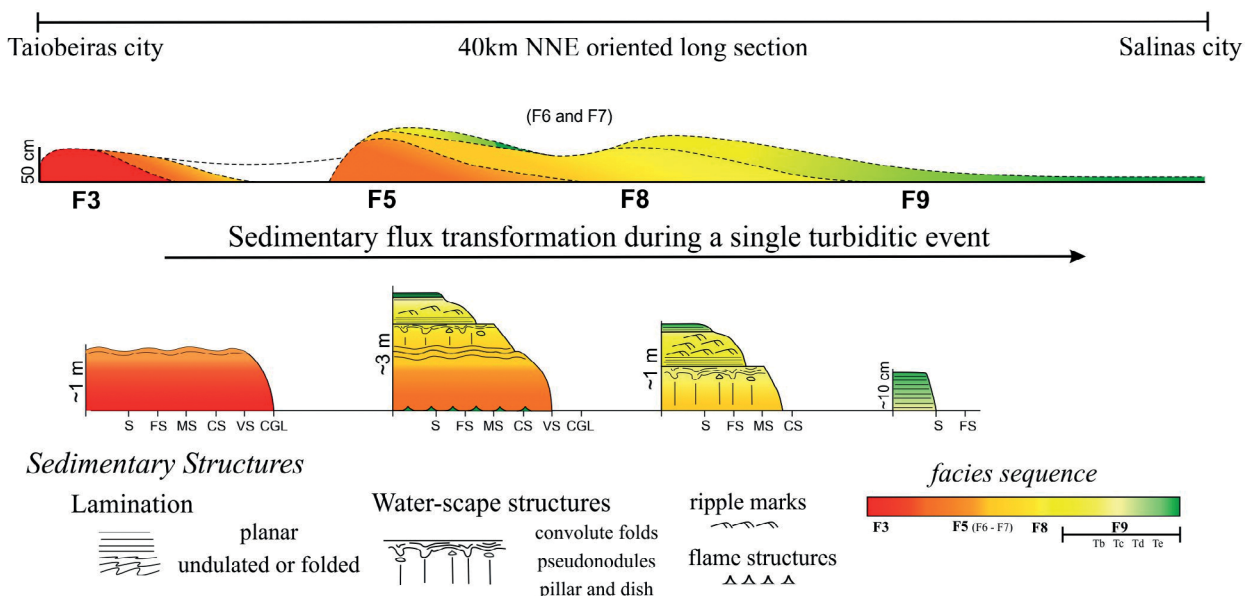


Figure 12. Proposed spatial facies distribution and transformation along 40 km during a single turbiditic event.

deposited on top of intensively deformed strata, continue with various sandy turbidite pulses, and ends with F9 dominated successions. This succession reflects the energy decay, retraction, and reorganization of the system after a major seismic event (recorded by the chaotic bed), which probably triggered high-energy turbidite flows and introduced significant changes in the basin morphology. The 8m-thick cycles reflect successive events in the aftermath of seismic episodes of decreasing magnitude, whereas the 1.2 m-thick single turbiditic pulses as systematically documented in the literature since Bouma (1962).

The generation of classes 2 to 4 soft-sediment deformations recorded in the 25–60 m-thick successions was associated with an overall SE-directed mass motion, *i.e.*, at a high angle to the principal sediment transport direction and in the opposite sense of the orogenic front propagation.

Reproducing the main paleocurrent vector indicated by ripples, the SE-directed moving slumps are probably a consequence of piggy-back propagation of the thrust front. As deformation progressed, newly nucleated thrusts and associated folds emerged in the west side of the basin, enhancing local slopes, giving rise to SE-moving slumps, and generating new obstacles for the turbiditic currents (Fig. 16). Furthermore, as emphasized by Tinterri & Magalhães (2011), the interaction of the turbiditic currents with the irregular morphology of a basin in process of closure creates the conditions for their partition in a basal dense flow and an upper turbulent flow, followed by the decoupling of the latter. The basal flow is in general not influenced by obstacles, eroding them away. This is, however, not the case of turbulent upper flow. The dispersion of the ripple paleocurrent data shown on Figure 6 may reflect the sinuous trajectories of decoupled turbulent

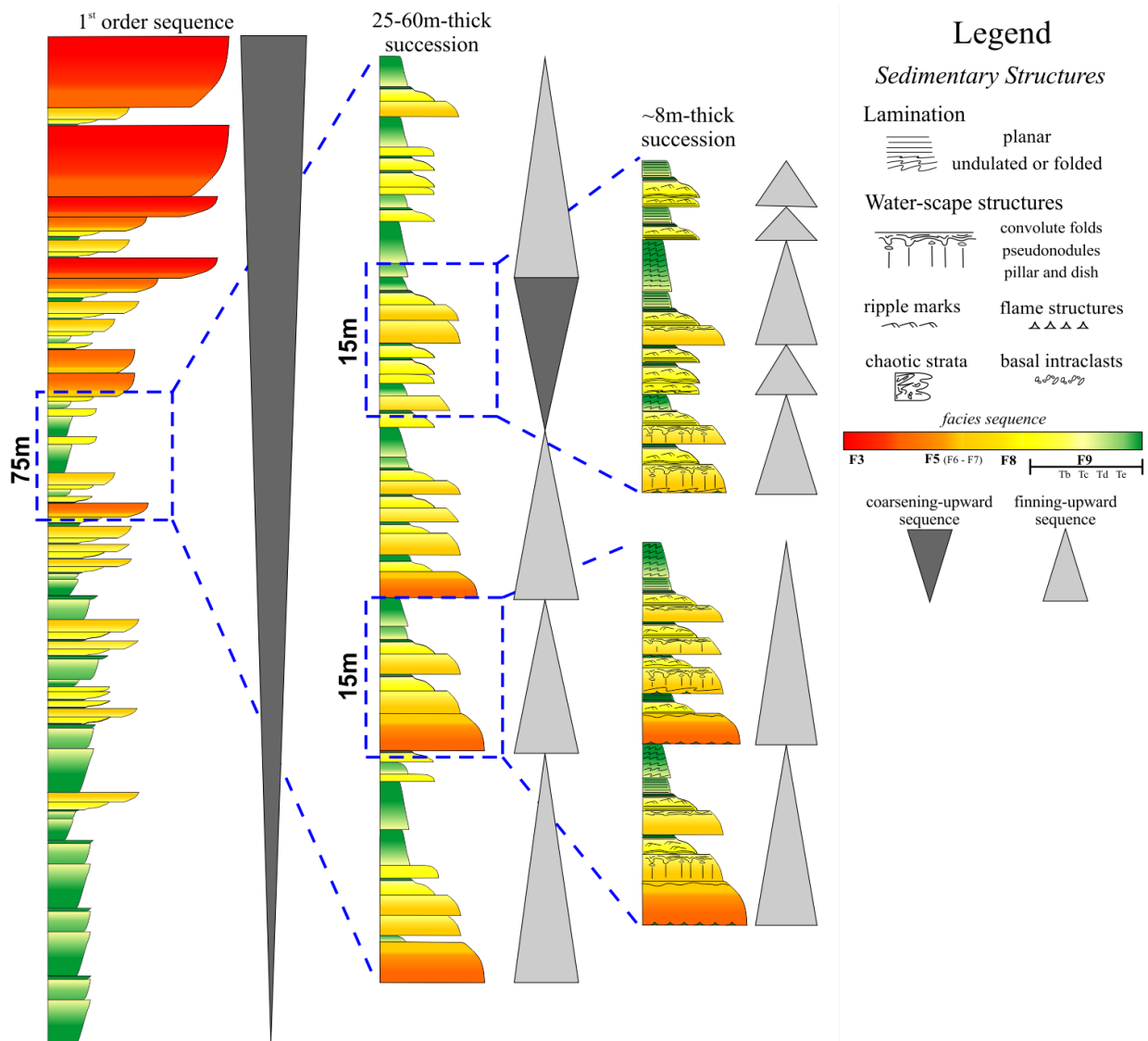


Figure 14. Diagram displaying three orders of sedimentary basin-fill cycles.

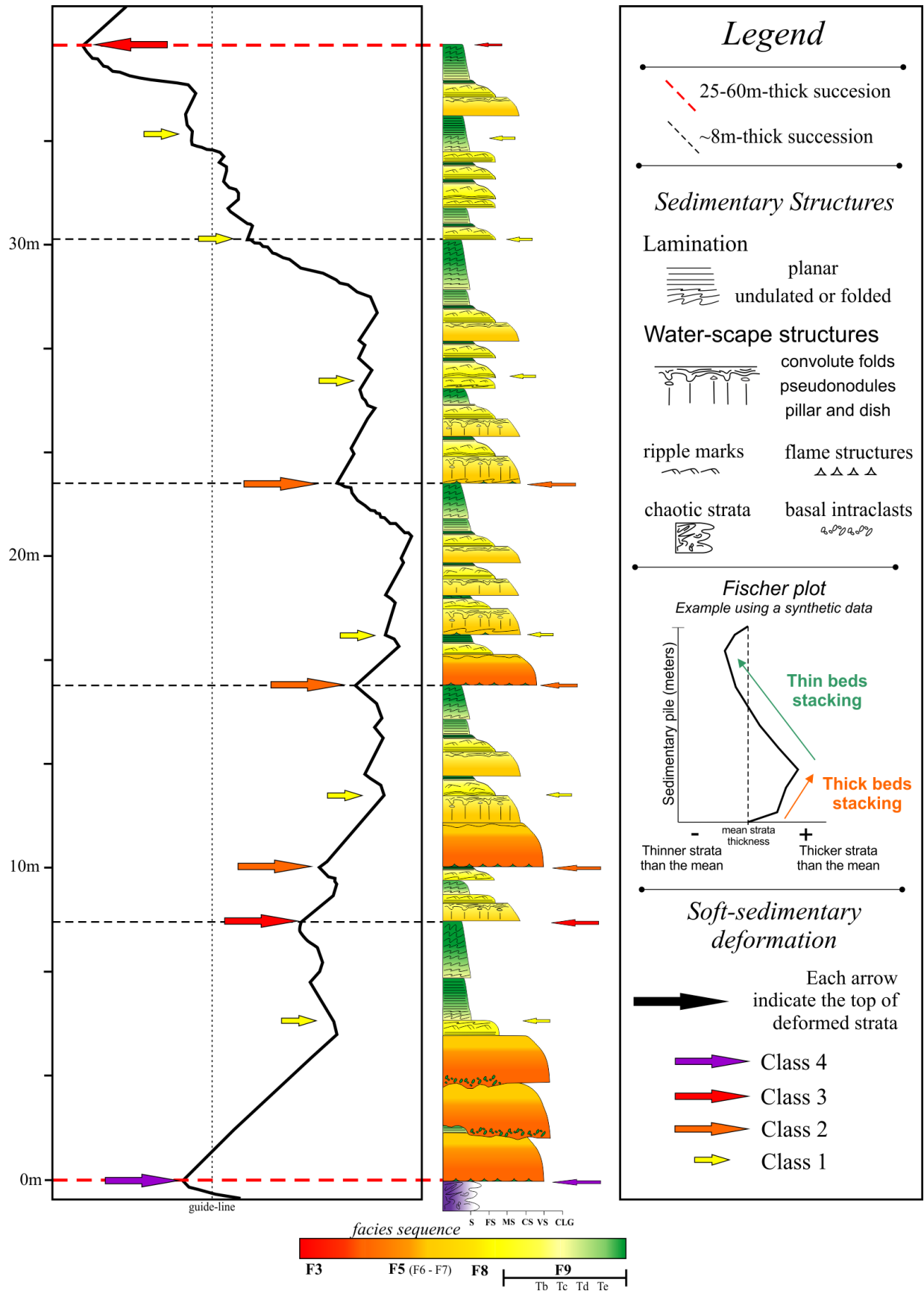


Figure 15. 25–60 m-thick cycle of the Salinas Formation and its typical stacking pattern, showing the tendency of fining-upward and decrease of the intensity of syn-sedimentary deformation to the top of the sequence.

flows, recorded by the F9 lithofacies assemblages. Again, their preferred SE-direction might be a response to obstacles located mainly in the west side of the basin.

DISCUSSION AND CONCLUSIONS

Some implications of the data and interpretations presented here demand a discussion in the light of the literature on the Araçuaí orogen and syn-orogenic basins in general. The first concerns the nature of the Salinas basin, which shares many attributes with the various types of pro- and retro-foreland basins. Foreland or downwarp basins are formed on a subsiding lithosphere, flexed under an encroaching dynamic load represented by an advancing orogenic wedge (Dickinson 1974, Miall 1995, Ingersoll 2012, Allen *et al.* 2015). The Salinas basin differs from them essentially in the geological setting and subsidence mechanism. The Salinas Formation occurs in a domain of the internal sector of the Araçuaí orogen that follows its suture zone, representing thus a remnant of the Macaúbas basin under continuous closure. In this respect, the Salinas basin differs from foreland basins, which are not residual and can migrate as the orogenic load advances (Ingersoll 2012, Ingersoll *et al.* 1995). However, the tectonic processes we supposed to have been active in the Salinas basin are essentially the same that take place in foreland piggy-back basins and wedge-top domains of down-warp basins in general (Ingersoll 2012, Ingersoll *et al.* 1995). Thus, the Salinas basin is similar to the foreland Proto-Adriatic basin of the Northern Apennines (Marnoso-Arenacea turbidites) (Tinterri & Magalhães 2011, Magalhaes & Tinterri 2010), Aínsa-Jaca basin, Pyrenees, Spain (Hecho Group turbidites) (Caja *et al.* 2010, Remacha & Fernández 2003), Punta Barrosa, Chilean Andes (Romans *et al.* 2011, Hubbard *et al.* 2008, 2010), and Peira Cava basin, French Alps (Annot Sandstone) (Tinterri *et al.* 2016, Cunha *et al.* 2017). Its best analogs are, however,

remnant basins represented, for instance, by the present-day Bengal and Indus fans (Ingersoll *et al.* 1995, 2003), and the Carboniferous Jackfork Formation of the Ouachita Mountains, United States. As pointed out by Moiola and Shanmugam (1984), the Jackfork basin was an elongated trough developed between the colliding margins of North America and Africa and filled with submarine fans that prograded along its axis. The resulting turbidite succession characterizes a typical coarsening upward 1st-order sequence, marking the suture between the two terranes. An intriguing aspect of the Salinas Turbidites is their provenance primarily from the Rio Doce magmatic arc (Lima *et al.* 2002, Pedrosa-Soares *et al.* 2008, Costa 2018). Authors devoted to the study of the Rio Doce arc postulated that it terminates around 16°30' South Lat. in the central portion of the Araçuaí orogen (Fig. 1). In fact, the northernmost occurrences of the G1 Supersuite granitic rocks and volcano-sedimentary rocks of the Rio Doce Group, which together form the arc assemblage (Tedeschi *et al.* 2016, Gonçalves *et al.* 2014, 2016), are located c.150 km to the east and southeast of the Salinas Formation exposures. Knowing that the Salinas basin was fed from the north, a complex source-sink linkage must have been established in the northern portion of the orogen in development. A possible solution here would involve an efficient drainage system flowing north and filling a depocenter located in the region of the present-day Rio Pardo valley. From this temporary accumulation site, the sediments would be then captured by dense flows and carried southwestwards into the Salinas trough (Fig. 17).

We also observe the lack of lateral feeding systems in the studied sector of the Salinas basin. Smaller transverse fans have been documented almost in all basin examples mentioned above. Their absence in the studied sections can be explained by both the spatial limitation of our observations and low preservation potential of these elements in the present level of exposure of the Araçuaí orogen.

In sum, our investigation led to following conclusions:

1. the syn-orogenic Salinas Formation consists of a succession of the following turbidite facies and facies assemblages: clast-supported conglomerates (F3), intraclastic breccias and normally graded sandstones (F5), cross-bedded sandstones (F6), massive sandstones (F8), sandstone with ripples, interlaminated sandstones and pelites, and laminated pelites (F9). These facies represent deposits of proximal channel bars (F3), channel-lobe transition (F5, F6), sand-lobes (F8), and basin plain (F9) of a turbidite fan system;
2. paleocurrent vectors obtained from conglomerate clast imbrications and sole marks indicate flow preferentially towards S35°W, the principal sediment transport direction along the axis of the Salinas basin. Paleocurrent vectors

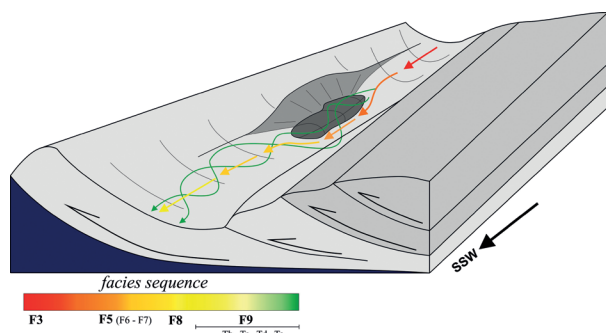


Figure 16. 3-D schematic model displaying the generation of new obstacles for the turbiditic currents during the progressive tectonic deformation.

- obtained from ripples show a relatively large dispersion and a bimodal distribution around S55°E (main vector) and S70°W;
3. soft-sediment deformation (SSD) affected all lithofacies. Four classes of SSD-structures were discriminated based on the amount of lateral displacement and rock volume involved. These are: water-escape structures (class 1); slightly deformed depositional and post-depositional features (class 2); faults and folds (class 3); and chaotic beds (class 4). Class 1 and 2 structures result from endogenic processes, whereas elements of class 3 and 4 very likely initiated by seismic shocks;
 4. the Salinas Formation as a whole comprises a coarsening upward 1st-order sequence, which encompasses
 5. four lower rank successions, three of them of fining upward character;
 6. the 1st-order sequence reflects the southwest-south progradation of the turbidite fan system along the axis of Salinas basin, a remnant of the precursor Macaúbas gulf in process of closure;
 7. the interplay between tectonic processes in the syn-orogenic Salinas basin is especially well recorded by the 25–60 m-thick fining-up, successions, which initiate with high energy turbidite events in the aftermath of

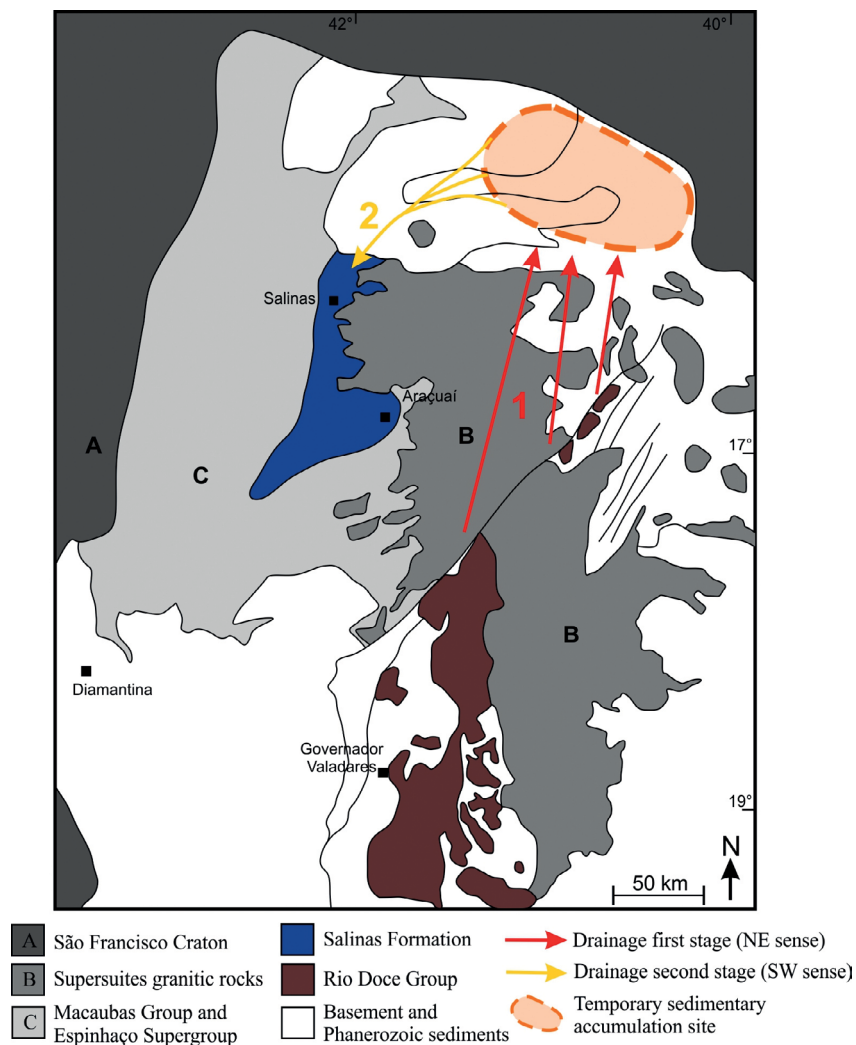


Figure 17. Simplified geological map showing the spatial distribution of the Salinas Formation and the Rio Doce Group, as well as the hypothetical two systems of drainage and the sedimentary depocenter before filling the Salinas basin.

a major seismic episode (represented by chaotic beds and slumps), follows with other turbiditic events of decreasing energy, and ends with the deposition of finer-grained facies. The middle and upper portions of these sequences reflects the energy decay and reorganization of basin morphology after a major deformation event;

8. the exceptional degree of preservation and high quality of the exposures make the Salinas Formation type area in northern Araçuaí orogen an excellent natural lab for unraveling the relationships between tectonics and sedimentation in syn-orogenic basins.

ACKNOWLEDGEMENTS

The authors are grateful to Marcos Fetter, Leonardo Siqueira, Pedro Pires, Rogerio Cunha and Roberto D'Ávila for their assistance on the field and discussions. This research was funded by Petrobras (Petroleo Brasileiro S.A.), Rede Geotectônica da Petrobras and CNPq (F.F.Alkmim Grant # 308045/2013-0). Comments and guidance from Editor-in-chief Claudio Riccomini, Associate Editor Carlos Alvarenga and two anonymous reviewers are gratefully acknowledged. They significantly improved the original manuscript.

REFERENCES

- Alkmim F.F., Kuchenbecker M., Reis H.L., Pedrosa-Soares A.C. 2017. The Araçuaí Belt. In: Heilbron M., Cordani U.G., Alkmim F.F. (Eds.), *São Francisco Craton, Eastern Brazil. Tectonic Genealogy of a Miniature Continent*. New York: Springer, p. 255-276.
- Alkmim F.F., Marshak S., Pedrosa-Soares A.C., Peres G.G., Cruz S.C.P., Whittington A. 2006. Kinematic evolution of the Araçuaí-West Congo orogen in Brazil and Africa: Nutcracker tectonics during the Neoproterozoic assembly of Gondwana. *Precambrian Research*, **149**(1-2):43-64. <https://doi.org/10.1016/j.precamres.2006.06.007>
- Alkmim F.F., Pedrosa-Soares A.C., Noce C.M., Cruz S.C.P. 2007. Sobre a evolução tectônica do orógeno Araçuaí-Congo Ocidental. *Revista Geonomos*, **15**(1):25-43. <http://dx.doi.org/10.18285/geonomos.v15i1.105>
- Allen J.R.L. 1980. Sand waves: a model of origin and internal structure. *Sedimentary Geology*, **26**(4):281-328. [https://doi.org/10.1016/0037-0738\(80\)90022-6](https://doi.org/10.1016/0037-0738(80)90022-6)
- Allen J.R.L. 1984. *Developments in Sedimentology*, 30. Amsterdam, Elsevier, 294 p.
- Allen P.A., Eriksson P.G., Alkmim F.F., Betts P.G., Catuneanu O., Mazumder R., Meng Q., Young G.M. 2015. *Classification of basins, with special reference to Proterozoic examples*. London, Geological Society of London, Memoirs, 43.
- Amy L.A., Talling P.J., Peakall J., Wynn R.B., Arzola Thynne R.G. 2005. Bed geometry used to test recognition criteria of turbidites and (sandy) debrites. *Sedimentary Geology*, **179**(1):163-174. <http://dx.doi.org/10.1016/j.sedgeo.2005.04.007>
- Bosellini A., Mutti E., Ricci Lucchi F. 1989. *Rocce e successioni sedimentarie*. Torino, Scienze della Terra – UTET, 395 p.
- Bouma A.H. 1962. *Sedimentology of some flysch deposits*. A graphic approach to facies interpretation. Amsterdam, Elsevier, 168 p.
- Caja M.A., Marfil R., Garcia D., Remacha E., Morad S., Mansurbeg H., Amorosi A., Martínez-Calvo C., Lahoz-Beltrá R. 2010. Provenance of siliciclastic and hybrid turbiditic arenites of the Eocene Hecho Group, Spanish Pyrenees: implications for the tectonic evolution of a foreland basin. *Basin Research*, **22**(2):157-180. <https://doi.org/10.1111/j.1365-2117.2009.00405.x>
- Cobra R.Q. 1970. *Geologia da Área da SUDENE ao sul do Paralelo 16*. Recife, Divisão de Geologia SUDENE.
- Costa F.G.D. 2018. *Controles tectônicos na sedimentação e empilhamento estratigráfico da Formação Salinas, Orógeno Araçuaí*. MG. Dissertation, Escola de Minas, Universidade Federal de Ouro Preto, Ouro Preto, 166 p.
- Cunha R.S., Tintneri R., Muzzi Magalhães P. 2017. Annot sandstone in the Peira Cava basin: Na example of an asymmetric facies distribution in a confined turbidite system (SE France). *Marine and Petroleum Geology*, **87**:60-79. <http://dx.doi.org/10.1016/j.marpetgeo.2017.04.013>
- D'Ávila R.S.F., Arienti L.M., Aragão M.A.N.F., Vesely F.F., Santos S.F., Voelcker H.E., Viana A.R., Kowsmann R.O., Moreira J.L.P., Coura A.P.P., Paim P.S.G., Matos R.S., Machado L.C.R. 2008. Ambientes Marinhos Profundos: sistemas turbidíticos. In: Silva A.J.C.L.P., Aragão M.A.N.F., Magalhães A.J.C. (Eds.), *Ambientes de sedimentação siliciclástica do Brasil*. São Paulo, Beca, p. 244-301.
- Dickinson W.R. 1974. Tectonics and sedimentation. *Special Publication of SEPM*, **22**:1-27. <https://doi.org/10.2110/pec.74.22>
- Graham J. 1988. Collection and analysis of field data. In: Tucker M. (Ed.), *Techniques in sedimentology*. Oxford, Blackwell Scientific Publications, p. 5-62.
- Gonçalves L., Alkmim F.F., Pedrosa-Soares A.C., Dussin I.A., Valeriano C.M., Lana C., Tedeschi M. 2016. Granites of the intracontinental termination of magmatic arc: an example from the Ediacaran Araçuaí orogen, southeastern Brazil. *Gondwana Research*, **36**:439-458. <http://dx.doi.org/10.1016/j.gr.2015.07.015>
- Gonçalves L., Farina F., Lana C., Pedrosa-Soares A.C., Alkmim F.F., Nalini Jr. H.A. 2014. New U-Pb ages and lithochemical attributes of the Ediacaran Rio Doce magmatic arc, Araçuaí confined orogen, southeastern Brazil. *Journal of South American Earth Sciences*, **52**:129-148. <http://dx.doi.org/10.1016/j.jsames.2014.02.008>
- Harms J.C., Southard J.B., Spearing D.R., Walker R.G. 1975. Conglomerate: sedimentary structures and facies models. *Special Publications of SEPM*, p. 133-161.
- Hubbard S.M., Fildani A., Romans B.W., Covault J.A., McHargue T.R. 2010. High-relief slope clinoform development: insights from outcrops, Magallanes basin, Chile. *Journal of Sedimentary Research*, **80**(5):357-375. <https://doi.org/10.2110/jsr.2010.042>
- Hubbard S.M., Romans B.W., Graham S.A. 2008. Deep-water foreland basin deposits of the Cerro Toro Formation, Magallanes basin, Chile: architectural elements of a sinuous basin axial channel belt. *Sedimentology*, **55**(5):1333-1359. <https://doi.org/10.1111/j.1365-3091.2007.00948.x>

- Ingersoll R.V. 2012. Tectonics of sedimentary basins, with revised nomenclature. In: Busby C., Azor A. (Eds.), *Tectonics of Sedimentary Basins: Recent Advances*. Oxford, Blackwell, p. 3-43.
- Ingersoll R.V., Dickinson W.R., Graham A. 2003. Remnant-ocean submarine fans: Largest sedimentary system on Earth. In: Chan M.A., Archer A.W. (Eds.), *Extreme depositional environments: mega end members in geologic time*. Geological Society of America Special Paper, **370**, p. 191-208.
- Ingersoll R.V., Graham A., Dickinson W.R. 1995. Remnant ocean basins. In: Busby C., Ingersoll R.V. (Eds.), *Tectonics of sedimentary basins*. Oxford, Blackwell Science, p. 363-391.
- Karfunkel J., Pedrosa-Soares A.C., Dossin I.A. 1985. O Grupo Macaúbas em Minas Gerais, revisão dos conhecimentos. In: Simpósio de Geologia, 3., MG. Anais... p. 45-59.
- Kuchenbecker M. 2014. *Relações entre coberturas do Cráton do São Francisco e bacias situadas em orógenos marginais: O Registro de datações U-Pb de grãos detríticos e suas implicações geotectônicas*. Thesis, Instituto de Geociências Universidade Federal de Minas Gerais, Belo Horizonte, 163 p.
- Lima S.A.A., Martins-Neto M.A., Pedrosa-Soares A.C., Cordani U.G., Nutman A. 2002. A Formação Salinas na área-tipo, NE de Minas Gerais: uma proposta de revisão da estratigrafia da Faixa Araçuaí com base em evidências sedimentares, metamórficas e idades U-Pb SHRIMP. *Revista Brasileira de Geociências*, **32**(4):491-500.
- Magalhaes P.M., Tinterri R. 2010. Stratigraphy and depositional setting of slurry and contained (reflected) beds in the Marnoso-arenacea Formation (Langhian-Serravallian) Northern Apennines, Italy. *Sedimentology*, **57**(7):1685-1720. <https://doi.org/10.1111/j.1365-3091.2010.01160.x>
- Marshak S., Alkmim F.F., Whittington A., Pedrosa-Soares A.C. 2006. Extensional collapse in the Neoproterozoic Araçuaí orogen, eastern Brazil: a setting for reactivation of asymmetric crenulation cleavage. *Journal of Structural Geology*, **28**(1):129-147. <http://doi.org/10.1016/j.jsg.2005.09.006>
- Miall A.D. 1990. *Principles of sedimentary basin analysis*. New York, Springer-Verlag, 668 p.
- Miall A.D. 1995. Collision-related foreland basins. In: Busby C., Ingersoll R.V. (Eds.), *Tectonics of sedimentary basins*. Oxford, Blackwell Science, p. 393-424.
- Middleton G.V., Hampton M.A. 1973. Sediment gravity flows: mechanics of flow and deposition. In: Middleton G.V., Bouma A.H. (Eds.), *Turbidites and Deep-water Sedimentation*. Los Angeles, SEPM Pacific Section, p. 1-38.
- Moiola R.J., Shanmugam G. 1984. Submarine fan sedimentation, Ouachita Mountains, Arkansas and Oklahoma. *AAPG Database*, Gulf Coast Association of Geological Societies Transactions, **34**, p. 175-182.
- Moretti M., Sabato L. 2007. Recognition of trigger mechanisms for soft-sediment deformation in the Pleistocene lacustrine deposits of the Sant'Arcangelo Basin (Southern Italy): Seismic shock vs. overloading. *Sedimentary Geology*, **196**(1-4):31-45. <https://doi.org/10.1016/j.sedgeo.2006.05.012>
- Mutti E. 1977. Distinctive thin-bedded turbidite facies and related depositional environments in the Eocene Hecho Group (South-central Pyrenees, Spain). *Sedimentology*, **24**(1):107-131. <https://doi.org/10.1111/j.1365-3091.1977.tb00122.x>
- Mutti E. 1992. *Turbidite sandstone*. San Donato Milanese, AGIP, Instituto di Geologia, Università di Parma, 275 p.
- Mutti E., Bernoulli D., Lucchi F.R., Tinterri R. 2009. Turbidites and turbidity currents from Alpine 'flysch' to the exploration of continental margins. *Sedimentology*, **56**(1):267-318. <https://doi.org/10.1111/j.1365-3091.2008.01019.x>
- Mutti E., Davoli G., Tinterri R., Zavala C. 1996. The importance of ancient fluvio-deltaic system dominated by catastrophic flooding in tectonically active basins. *Memorie di Scienze Geologiche*, **48**:233-291.
- Mutti E., Tinterri R., Benevelli G., di Biase D., Cavanna G. 2003. Deltaic, mixed and turbidite sedimentation of ancient foreland basins. *Marine and Petroleum Geology*, **20**(6):733-755. <http://dx.doi.org/10.1016/j.marpetgeo.2003.09.001>
- Mutti E., Tinterri R., Remacha E., Mavilla N., Angella S., Fava L. 1999. An Introduction to the Analysis of Ancient Turbidite Basins from an Outcrop Perspective. *AAPG Continuing Education Course Note*, **39**, 74 p.
- Catuneanu O., Martins-Neto M., Eriksson P.G. 2005. Precambrian sequence stratigraphy. *Sedimentary Geology*, **176**(1-2):67-95. <https://doi.org/10.1016/j.sedgeo.2004.12.009>
- Owen G. 2003. Load structures: gravity-driven sediment mobilization in the shallow subsurface. In: Van Rensbergen P., Hillis R.R., Maltman A.J., Morely C.K. (Eds.), *Subsurface Sediment Mobilization*. Geological Society of London, Special Publication, **216**:21-34.
- Owen G., Moretti M. 2011. Identifying triggers for liquefaction-induced soft-sediment deformation in sands. *Sedimentary Geology*, **235**(3-4):141-147. <https://doi.org/10.1016/j.sedgeo.2010.10.003>
- Owen G., Moretti M., Alfaro P. 2011. Recognising triggers for soft-sediment deformation: Current understanding and future directions. *Sedimentary Geology*, **235**(3-4):133-140. <http://dx.doi.org/10.1016/j.sedgeo.2010.12.010>
- Pedrosa-Soares A.C. 1995. *Potencial aurífero do Vale do Araçuaí, MG: história da exploração, geologia e controle tectono-metamórfico*. Thesis, Instituto de Geociências, Universidade de Brasília, Brasília, 177 p.
- Pedrosa-Soares A.C., Alkmim F.F., Tack L., Noce C.M., Babinski M., Silva L.C., Martins-Neto M. 2008. Similarities and differences between the Brazilian and African counterparts of the Neoproterozoic Araçuaí-West Congo Orogen. In: Pankhurst J.R., Trouw R.A.J., Brito Neves B.B., De Wit M.J. (Eds.), *West Gondwana: Pre-Cenozoic Correlations across the South Atlantic Region*. London, Geological Society of London, Special Publications, **294**:153-172.
- Pedrosa-Soares A.C., Babinski M., Noce C., Martins M., Queiroga G., Vilela F. 2011. The Neoproterozoic Macaúbas Group, Araçuaí orogen, SE Brazil. *Memoirs*, **36**(1):523-534. <http://dx.doi.org/10.1144/M36.49>
- Pedrosa-Soares A.C., Noce C.M., Alkmim F.F., Silva L.C.D., Babinski M., Cordani U., Castañeda C. 2007. Orógeno Araçuaí: síntese do conhecimento 30 anos após Almeida 1977. *Revista Geonomos*, **15**(1):1-16. <http://dx.doi.org/10.18285/geonomos.v15i1.103>
- Pedrosa-Soares A.C., Noce C.M., Vida P., Monteiro R.L.B.P., Leonardos O.H. 1992. Toward a new tectonic model for the late proterozoic Araçuaí (SE Brazil)-West Congolian (SW Africa) belt. *Journal of South American Earth Sciences*, **6**(1-2):33-47. [http://dx.doi.org/10.1016/0895-9811\(92\)90015-Q](http://dx.doi.org/10.1016/0895-9811(92)90015-Q)
- Pedrosa-Soares A.C., Noce C.M., Wiedemann C.M., Pinto C.P. 2001. The Araçuaí-West-Congo Orogen in Brazil: an overview of a confined orogen formed during Gondwanaland assembly. *Precambrian Research*, **110**(1):307-323. [http://dx.doi.org/10.1016/S0301-9268\(01\)00174-7](http://dx.doi.org/10.1016/S0301-9268(01)00174-7)
- Pedrosa-Soares A.C., Wiedemann-Leonardos C.M. 2000. Evolution of the Araçuaí Belt and its connection to the Ribeira Belt, eastern Brazil. In: Cordani U.G., Milani E.J., Thomaz Filho A., Campos D.A. (Eds.), *Tectonic Evolution of South America*, **31**:265-310.
- Peixoto E., Alkmim F.F., Pedrosa-Soares A., Lana C., Chaves A.O. 2018. Metamorphic record of collision and collapse in the Ediacaran-Cambrian Araçuaí orogen, SE-Brazil: Insights from P-T pseudosections and monazite dating. *Journal of Metamorphic Geology*, **36**(2):147-172. <https://doi.org/10.1111/jmg.12287>

- Peixoto E., Pedrosa-Soares A.C., Alkmim F.F., Dussin I.A. 2015. A suture-related accretionary wedge formed in the Neoproterozoic Araçuaí orogen (SE Brazil), during western Gondwanaland assembly. *Gondwana Research*, **27**:878-896. <http://dx.doi.org/10.1016/j.gr.2013.11.010>
- Potter P.E., Pettijohn F.J. 1977. *Paleocurrents and Basin Analysis*. Berlin, Springer-Verlag, 425 p.
- Queiroga G.N., Pedrosa-Soares A.C., Noce C.M., Alkmim F.F., Pimentel M.M., Dantas E., Martins M., Castañeda C., Suita M.T.F., Prichard H. 2007. Age of the Ribeirão da Folha ophiolite, Araçuaí Orogen: The U-PB zircon (La-ICPMS) dating of a plagiogranite. *Geonomos*, **15**(1):61-65. <http://dx.doi.org/10.18285/geonomos.v15i1.107>
- Remacha E., Fernández L.P. 2003. High-resolution correlation patterns in the turbidite systems of the Hecho Group (South-Central Pyrenees, Spain). *Marine and Petroleum Geology*, **20**(6-8):711-726. <https://doi.org/10.1016/j.marpetgeo.2003.09.003>
- Ricci Lucchi F., Valmori E. 1980. Basin-wide turbidites in a Miocene over supplied deep-sea plain: a geometrical analysis. *Sedimentology*, **27**(3):241-270. <https://doi.org/10.1111/j.1365-3091.1980.tb01177.x>
- Romans B.W., Fildani A., Hubbard S.M., Covault J.A., Fosdick J.C., Graham S.A. 2011. Evolution of deep-water stratigraphic architecture, Magallanes Basin, Chile. *Marine and Petroleum Geology*, **28**(3):612-628. <https://doi.org/10.1016/j.marpetgeo.2010.05.002>
- Rossetti D.F. 1999. Soft-sediment deformation structures in late Albian to Cenomanian deposits, São Luís Basin, northern Brazil: evidence for palaeoseismicity. *Sedimentology*, **46**(6):1065-1081. <https://doi.org/10.1046/j.1365-3091.1999.00265.x>
- Santos R.F. 2007. *A Formação Salinas da Faixa Araçuaí, MG: Acervo Estrutural e Significado Tectônico*. Dissertation, Universidade Federal de Ouro Preto, Departamento de Geologia, Ouro Preto, 120 p.
- Santos R.F., Alkmim F.F., Pedrosa-Soares A.C. 2009. A Formação Salinas, Orógeno Araçuaí (MG): história deformacional e significado tectônico. *Revista Brasileira de Geociências*, **39**(1):81-100.
- Shanmugam G. 2017. Global case studies of soft-sediment deformation structures (SSDS): Definitions, classifications, advances, origins, and problems. *Journal of Palaeogeography*, **6**(4):251-320. <https://doi.org/10.1016/j.jop.2017.06.004>
- Shanmugam G., Muiola R.J. 1988. Submarine fans: Characteristics, models, classification, and reservoir potential. *Earth-Science Reviews*, **24**(6):383-428. [http://dx.doi.org/10.1016/0012-8252\(88\)90064-5](http://dx.doi.org/10.1016/0012-8252(88)90064-5)
- Tack L., Wingate M.T.D., Liégeois J.P., Fernandez-Alonso M., Deblond A. 2001. Early Neoproterozoic magmatism (1000–910 Ma) of the Zadinian and Mayumbian Groups (Bas-Congo): onset of Rodinian rifting at the western edge of the Congo Craton. *Precambrian Research*, **110**:277-306.
- Talling P.J. 2001. On the frequency distribution of turbidite thickness. *Sedimentology*, **48**(6):1297-1329. <https://doi.org/10.1046/j.1365-3091.2001.00423.x>
- Talling P.J., Amy L.A., Wynn R.B. 2007. New insight into the evolution of large-volume turbidity currents: comparison of turbidite shape and previous modelling results. *Sedimentology*, **54**(4):737-769. <https://doi.org/10.1111/j.1365-3091.2007.00858.x>
- Tedeschi M., Novo T., Pedrosa-Soares A., Dussin I., Tassinari C., Silva L.C., Gonçalves L., Alkmim F.F., Lana C., Figueiredo C., Dantas E., Medeiros S., Campos C., Corrales F., Heilbron M. 2016. The Ediacaran Rio Doce magmatic arc revisited (Araçuaí-Ribeira orogenic system, SE Brazil). *Journal of South American Earth Sciences*, **68**:167-186. <http://dx.doi.org/10.1016/j.jsames.2015.11.011>
- Tinterri R., Magalhaes P.M. 2011. Synsedimentary structural control on foredeep turbidites: An example from Miocene Marnoso-arenacea Formation, Northern Apennines, Italy. *Marine and Petroleum Geology*, **28**(3):629-657. <http://dx.doi.org/10.1016/j.marpetgeo.2010.07.007>
- Tinterri R., Magalhaes P.M., Tagliaferri A., Cunha R.S. 2016. Convolute laminations and load structures in turbidites as indicators of flow reflections and decelerations against bounding slopes. Examples from the Marnoso-arenacea Formation (northern Italy) and Annot Sandstones (southeastern France). *Sedimentary Geology*, **344**:382-407. <http://dx.doi.org/10.1016/j.sedgeo.2016.01.023>
- Walker R.G. 1975. Generalized facies models for resedimented conglomerates of turbidite association. *Geological Society of America Bulletin*, **86**(6):737-748. [https://doi.org/10.1130/0016-7606\(1975\)86%3C737:GFMFRC%3E2.0.CO;2](https://doi.org/10.1130/0016-7606(1975)86%3C737:GFMFRC%3E2.0.CO;2)
- Walker R.G. 1992. Turbidites and submarine fans. In: Walker R.G., James N.P. (Eds.), *Facies models response to sea-level changes*. Stittsville, Love Printing, p. 239-263.

